arXiv:astro-ph/0303272v1 12 Mar 2003

Element Abundances through the Cosmic Ages†

By MAX PETTINI[1]

[1] Institute of Astronomy, University of Cambridge
Madingley Road, Cambridge, UK

The horizon for studies of element abundances has expanded dramatically in the last ten years. Once the domain of astronomers concerned chiefly with stars and nearby galaxies, this field has now become a key component of observational cosmology, as technological advances have made it possible to measure the abundances of several chemical elements in a variety of environments at redshifts up to $z \simeq 4$, when the universe was in its infancy. In this series of lectures I summarise current knowledge on the chemical make-up of distant galaxies observed directly in their starlight, and of interstellar and intergalactic gas seen in absorption against the spectra of bright background sources. The picture which is emerging is one where the universe at $z = 3$ already included many of the constituents of today's galaxies—even at these early times we see evidence for Population I and II stars, while the 'smoking gun' for Population III objects may be hidden in the chemical composition of the lowest density regions of the intergalactic medium, yet to be deciphered.

1. Introduction

One of the exciting developments in observational cosmology over the last few years has been the ability to extend studies of element abundances from the local universe to high redshifts. Thanks largely to the new opportunities offered by the Keck telescopes, the Very Large Telescope facility at the European Southern Observatory, and most recently the Subaru telescope, we find ourselves in the exciting position of being able, for the first time, to detect and measure a wide range of chemical elements directly in stars, H II regions, cool interstellar gas and hot intergalactic medium, all observed when the universe was only $\sim 1/15$ of its present age. Our simple-minded hope is that, by moving back to a time when the universe was young, clues to the nature, location, and epoch of the first generations of stars may be easier to interpret than in the relics left today, some 12 Gyrs later. Furthermore, the metallicities of different structures in the universe and their evolution with redshift are key factors to be considered in our attempts to track the progress of galaxy formation through the cosmic ages.

In the last few years, work on chemical abundances at high redshifts has concentrated on four main components of the young universe: Active Galactic Nuclei (AGN), that is quasars (QSOs) and Seyfert galaxies; two classes of QSO absorption lines, the damped Lyα systems (DLAs) and the Lyα forest; and on galaxies detected directly via their starlight, also referred to as Lyman break galaxies. In these series of lectures I will review results pertaining to the last three; for abundance determinations in the emission line regions of AGN and associated absorbers I refer the interested reader to the excellent recent overview by Hamann & Ferland (1999).

† Lectures given at the XIII Canary Islands Winter School of Astrophysics *'Cosmochemistry: The Melting Pot of Elements'*. Available in electronic form from http://www.ast.cam.ac.uk/~pettini/canaries13

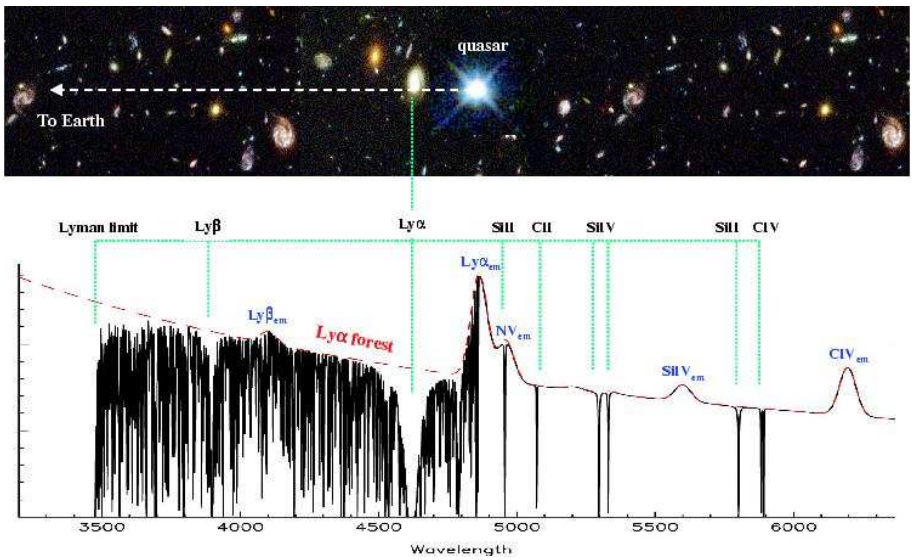

FIGURE 1. The technique of QSO absorption line spectroscopy is illustrated in this montage (courtesy of John Webb). QSOs are among the brightest and most distant objects known. On the long journey from its source to our telescopes on Earth, the light from a background QSO intercepts galaxies and intergalactic matter which happen to lie along the line of sight (and are therefore at lower absorption redshifts, $z_{\rm abs}$, than the QSO emission redshift, $z_{\rm em}$. Gas in these structures leaves a clear imprint in the spectrum of the QSO in the form of narrow absorption lines. The task of astronomers working in this field has been to relate the characteristics of the absorption lines to the properties of the intervening galaxies which are normally too faint to be detected directly.

1.1. *Some Basic Concepts*

For many years our knowledge of the distant universe relied almost exclusively on QSO absorption lines. It is only relatively recently that we have learnt to identify directly 'normal' galaxies; up until 1995 the only objects known at high z were QSOs and powerful radio galaxies. The technique of QSO absorption line spectroscopy, illustrated in Figure 1, is potentially very powerful. As we shall see, it allows accurate measurements of many physical properties of the interstellar medium (ISM) in galaxies and the intergalactic medium (IGM) between galaxies. The challenge, however, is to relate this wealth of data, which refer to gas along a very narrow sightline, to the global properties of the absorbers. In a sense, all the information we obtain from QSO absorption line spectroscopy is of an *indirect* nature; if we could detect the galaxies themselves, our inferences would be on a stronger empirical basis.

In deriving chemical abundances in QSO absorbers and high redshift galaxies, we shall make use of some of the same techniques which are applied locally to interpret the spectra of stars, cool interstellar gas and H II regions. These methods are discussed extensively in other articles in this volume, particularly those by Don Garnett, David Lambert, and Grazyna Stasinska, and will therefore not be repeated here. The derivation of ion column densities from the profiles and equivalent widths of interstellar absorption lines is discussed in a number of standard textbooks, as well as a recent volume in this series (Bechtold 2002).

When measuring element abundances in different astrophysical environments, we shall often compare them to the composition of the solar system determined either from photospheric lines in the solar spectrum or, preferably, from meteorites. The standard solar abundance scale continues to be refined; here we adopt the compilation by Grevesse & Sauval (1998) with the recent updates by Holweger (2001). We use the standard notation $[\mathrm{X/Y}] = \log(\mathrm{X/Y})_{\mathrm{obs}} - \log(\mathrm{X/Y})_{\odot}$ where $(\mathrm{X/Y})_{\mathrm{obs}}$ denotes the abundance of element X relative to element Y in the system under observation—be it stars, interstellar gas or the intergalactic medium—and $(\mathrm{X/Y})_{\odot}$ is their relative abundance in the solar system.

Furthermore, it is important to remember that when element abundances are measured in the interstellar gas of the Milky Way, it is usually found that $[\mathrm{X/H}] < 0$. This deficiency is not believed to be intrinsic, but rather reflects the proportion of heavy elements that has condensed out of the gas phase to form dust grains (and therefore no longer absorbs starlight via discrete atomic transitions). As discussed in the review by Savage & Sembach (1996), the 'missing' fraction varies from element to element, reflecting the ease with which different constituents of interstellar dust are either incorporated into the grains or released from them. In particular, O, N, S, and Zn show little affinity for dust and are often present in the gas in near-solar proportions; Si, Fe and most Fe-peak elements, on the other hand, can be depleted by large and varying amounts depending on the physical conditions—past and present—of the interstellar clouds under study.

Unless otherwise stated, we shall use today's 'consensus' cosmology (e.g. Turner 2002) with $H_0 = 65\,\mathrm{km\ s^{-1}\ Mpc^{-1}}$ (and hence $h = 0.65$), $\Omega_{\mathrm{baryons}} = 0.022\,h^{-2}$, $\Omega_{\mathrm{M}} = 0.3$, and $\Omega_{\Lambda} = 0.7$. Table 1 shows the run of look-back time with redshift for this cosmology. Note that with the above cosmological parameters the age of the universe is 14.5 Gyr, consistent with recent estimates of the ages of globular clusters (Krauss & Chaboyer 2001). When in these lecture notes we refer to 'high' redshifts we usually mean $z = 3 - 4$ which correspond to look-back times of 12–13 Gyr, when the universe had only 15–10% of its present age. Epochs when z was ≤ 1 are generally referred to as 'intermediate' or 'low' redshifts, even though they correspond to look-back times of up to about 60% of the current age of the universe.

Table 1. Lookback time vs. redshift in the adopted cosmology

Redshift	Lookback Time (Gyr)	Lookback time (t/t_{∞})
0	0	0
0.5	5.4	0.37
1	8.3	0.57
2	11.0	0.76
3	12.2	0.84
4	12.9	0.89
5	13.3	0.92
6	13.5	0.93
10	14.0	0.97
∞	14.5	1.00

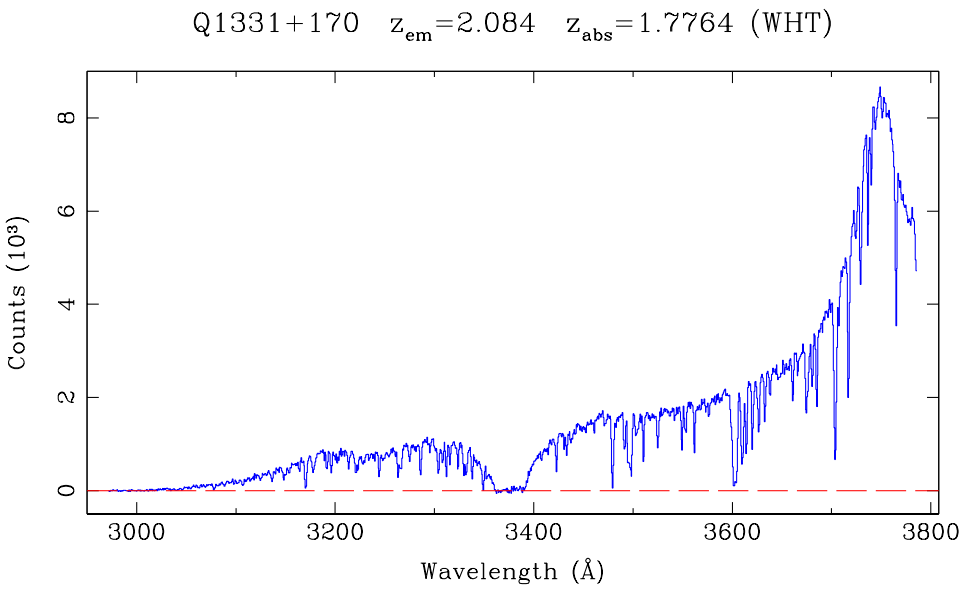

FIGURE 2. The strong absorption feature centred near 3375 Å in the near-ultraviolet (UV) spectrum of the bright QSO Q1331+170 is a good example of a damped Lyα line, in this case produced by a column density of neutral hydrogen atoms $N(\mathrm{H\ I}) = 1.5 \times 10^{21}\,\mathrm{cm}^{-2}$. This spectrum was recorded in the early 1990s with the Image Photon Counting System on the ISIS spectrograph of the 4.2 m William Herschel telescope on La Palma (Pettini et al. 1994).

2. Damped Lyα Systems

2.1. *What Are They?*

I am often asked this question, and the truthful answer is: "We do not know". Spectroscopically, DLAs are straightforward to identify (see Figure 2). The large equivalent widths and characteristic damping wings which signal column densities of absorbing neutral hydrogen in excess of $N(\mathrm{H\ I}) = 2 \times 10^{20}\,\mathrm{cm}^{-2}$ are easy to recognise even in spectra of moderate resolution and signal-to-noise ratio (significantly worse than those of the spectrum reproduced in Figure 2).

The galaxies producing DLAs, however, have proved difficult to pin down. Wolfe and collaborators, who were the first to recognise DLAs as a class of QSO absorbers of special significance for the study of the high redshift universe (e.g. Wolfe et al. 1986), proposed from the outset that they are the progenitors of present-day spiral galaxies, observed at a time when most of their baryonic mass was still in gaseous form. The evidence supporting this scenario, however, is mostly indirect. For example, Prochaska & Wolfe (1998) showed that the profiles of the metal absorption lines in DLAs are consistent with the kinematics expected from large, rotating, thick disks, but others have claimed that this interpretation is not unique (Haehnelt, Steinmetz, & Rauch 1998; Ledoux et al. 1998).

Imaging studies at high redshift are only now beginning to identify some of the absorbers (Prochaska et al. 2002; Møller et al. 2002). At $z < 1$, where the imaging is easier (an example is reproduced in Figure 3), it appears that DLA galaxies are a very 'mixed bag', which includes a relatively high proportion of low surface brightness and low luminosity galaxies (some so faint that they remain undetected in their stellar populations,

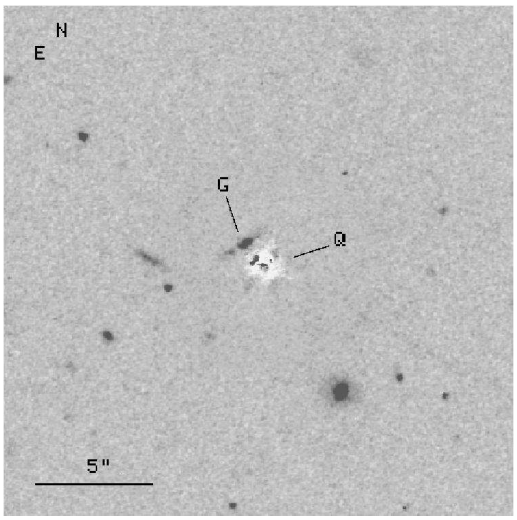

FIGURE 3. (Reproduced from Pettini et al. 2000a). WFPC2 F702W exposure of the field of Q0058+019 (PHL 938). A model point spread function has been subtracted from the QSO image (labelled 'Q'), revealing the presence of a galaxy (labelled 'G') approximately 1.2 arcseconds to the NE of the QSO position. Given its proximity, this is likely to be the damped Ly α absorber at $z = 0.61251$. Residual excess absorption of a diffraction spike cuts across the galaxy image. When this processing artifact is taken into account, the candidate absorber appears to be a low luminosity ($L \simeq 1/6\,L^*$) late-type galaxy seen at high inclination, $i \approx 65^\circ$, at a projected separation of $6\,h^{-1}$ kpc from the QSO sightline.

e.g. Steidel et al. 1997; Bouché et al. 2001), as well as more 'normal' spirals (Boissier, Péroux, & Pettini 2002).

Much was made in the early 1990s of the apparent correspondence between the neutral gas mass traced by DLAs at high redshift ($\Omega_{\rm DLA}\,h \simeq 1.2 \times 10^{-3}$, when expressed as a fraction of the critical density) and today's luminous stellar mass, leading to suggestions that the former are the material out of which the latter formed (e.g. Lanzetta 1993). However, the apparent decrease in $\Omega_{\rm DLA}$ from $z = 3$ to 0, upon which this picture was based, has not been confirmed with more recent and more extensive samples (Pettini 2001). As can be seen from Figure 4, current data are consistent with an approximately constant value $\Omega_{\rm DLA}$ over most of the Hubble time, and this includes the most recent estimates of $\Omega_{\rm H\ I}$ in the local universe from 21 cm surveys (Rosenberg & Schneider 2002; not shown in Figure 4). Perhaps DLAs pick out a particular stage in the evolution of galaxies, when their dimensions in high surface density of neutral gas are largest, and it may be the case that different populations of galaxies pass through this stage at different cosmic epochs.

2.2. *Why Do We Care?*

While we would obviously like to know more clearly which population(s) of galaxies DLAs are associated with, this issue does not detract from the importance of this class of QSO absorbers for studies of element abundances, for the following reasons.

First, with neutral hydrogen column densities N(H I)$\geq 2 \times 10^{20}$ cm^{-2}, DLAs are the 'heavy weights' among QSO absorption systems, at the upper end of the distribution of values of N(H I) which spans 10 orders of magnitude for all absorbers (see Figure 5).

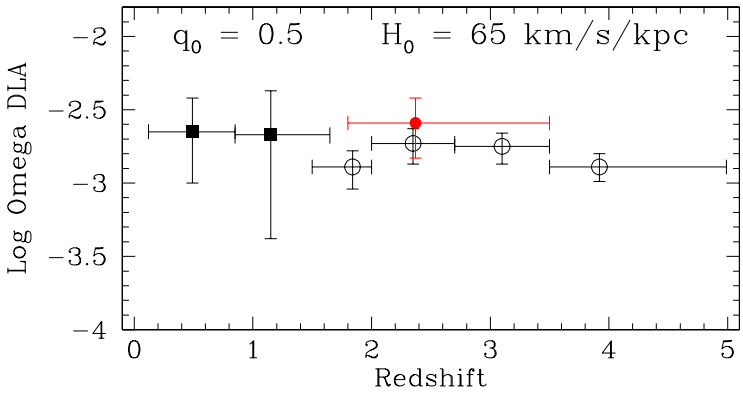

FIGURE 4. Recent estimates of the mass density of neutral gas traced by damped Lyα systems, expressed as a fraction of the critical density. The filled squares are from Rao & Turnshek (2000); the open circles from Storrie-Lombardi & Wolfe (2000) and from Péroux et al. (2002); while the filled circle is from the CORALS survey by Ellison et al. (2001).

Over this entire range, $f(N_{\rm H\ I})$—defined as the number of absorbing systems per unit redshift path per unit column density—can be fitted with a single power law of the form

$$f(N_{\rm H\ I}) = B \times N_{\rm H\ I}^{-\beta} \tag{2.1}$$

with $\beta \simeq 1.5$ (Tytler 1987; Storrie-Lombardi & Wolfe 2000). While the most numerous absorbers are those with the lowest column densities (a turn-over at low values of N(H I) has yet to be found), the high column densities of DLAs more than compensate for their relative paucity. More specifically, so long as $\beta < 2$, the integral of the column density distribution

$$\Omega_{\rm H\ I} = \frac{H_0}{c}\,\frac{\mu\, m_{\rm H}}{\rho_{\rm crit}} \int_{N_{\rm min}}^{N_{\rm max}} N\, f(N)\, dN = \frac{H_0}{c}\,\frac{\mu\, m_{\rm H}}{\rho_{\rm crit}}\,\frac{B}{2-\beta}\,\left(N_{\rm max}^{2-\beta} - N_{\rm min}^{2-\beta}\right) \tag{2.2}$$

is dominated by $N_{\rm max}$, i.e. by DLAs (Lanzetta 1993). In eq. (2.2), H_0 is the Hubble constant, c is the speed of light, $m_{\rm H}$ is the mass of the hydrogen atom, μ is the mean atomic weight per baryon ($\mu = 1.4$ for solar abundances; Grevesse & Sauval 1998) and $\rho_{\rm crit}$ is the closure density

$$\rho_{\rm crit} = \frac{3\,H_0^2}{8\,\pi\,G} = 1.96 \times 10^{-29} h^2\ {\rm g\ cm^{-3}} \tag{2.3}$$

where h is the Hubble constant in units of 100 km s^{-1} Mpc^{-1}.

As a consequence, the mean metallicity of DLAs is the closest measure we have of the global degree of metal enrichment of neutral gas in the universe at a given epoch, *irrespectively of the precise nature of the absorbers*, a point often emphasised by Mike Fall and his collaborators (e.g. Fall 1996). Of course this only applies if there are no biases which exclude any particular type of high redshift object from our H I census.

Second, it is possible to determine the abundances of a wide variety of elements in DLAs with higher precision than in most other astrophysical environments in the distant universe. In particular, echelle spectra obtained with large telescopes can yield abundance measures accurate to 10–20% (e.g. Prochaska & Wolfe 2002), because: (a) the damping wings of the Lyα line are very sensitive to the column density of H I; (b) several atomic transitions are often available for elements of interest; and (c) ionisation corrections are

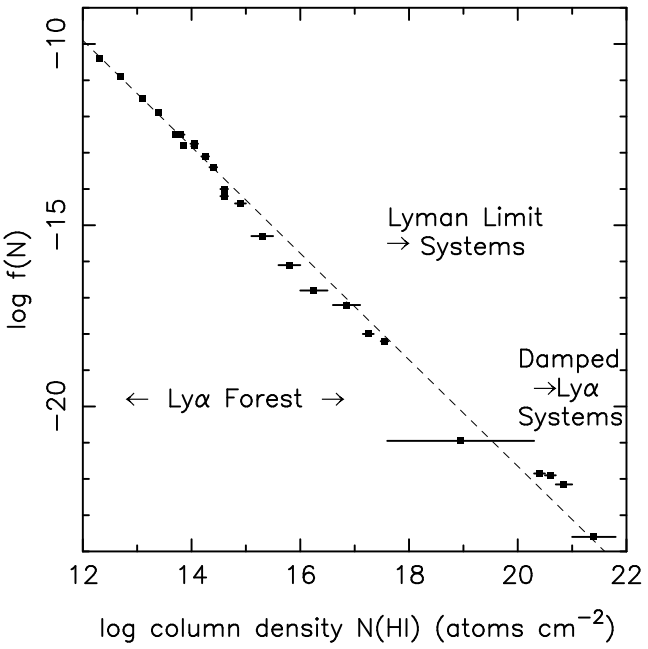

FIGURE 5. (Reproduced from Storrie-Lombardi & Wolfe 2000). The column density distribution function of neutral hydrogen for all QSO absorbers spans ten orders of magnitude, from $\log N(\mathrm{H\ I}) = 12$ to 22 and can be adequately described by a single power law $f(N_{\mathrm{H\ I}}) \propto N_{\mathrm{H\ I}}^{-1.5}$, shown by the dashed line.

normally small, because the gas is mostly neutral and the major ionisation stages are observed directly (Vladilo et al. 2001). Dust depletions can be a complication, but even these are not as severe in DLAs as in the local interstellar medium (Pettini et al. 1997a) and can be accounted for with careful analyses (e.g. Vladilo 2002a). Thus, abundance studies in DLAs complement in a very effective way the information provided locally by stellar and nebular spectroscopy and, as we shall see, can offer fresh clues to the nucleosynthesis of elements, particularly in metal-poor environments which are difficult to probe in the nearby universe. DLAs are also playing a role in the determination of the primordial abundances of the light elements, as discussed by Gary Steigman in this volume (see also Tytler et al. 2000 and Pettini & Bowen 2001).

2.3. *The Metallicity of DLAs*

Even before the advent of 8-10 m class telescopes, it was realised that the metal and dust content of DLAs could be investigated effectively by targeting a pair of (fortuitously) closely spaced multiplets, Zn II $\lambda\lambda$2025, 2062 and Cr II $\lambda\lambda$2056, 2062, 2066 (Meyer, Welty, & York 1989; Pettini, Boksenberg, & Hunstead 1990). The key points here are that while Zn is essentially undepleted in local diffuse interstellar clouds, Cr is mostly locked up in dust grains (Savage & Sembach 1996). Consequently, the ratio $N(\mathrm{Zn\ II})/N(\mathrm{H\ I})$ observed in DLAs, when compared with the solar abundance of Zn, yields a direct measure of the degree of metal enrichment (in H I regions Zn is predominantly singly ionised, and the ratios Zn I/Zn II and Zn III/Zn II are both $\ll 1$). On the other hand, a deficit—if one is found—of $N(\mathrm{Cr\ II})/N(\mathrm{Zn\ II})$ compared to the solar relative abundances of these two elements would measure the extent to which refractory elements have condensed into

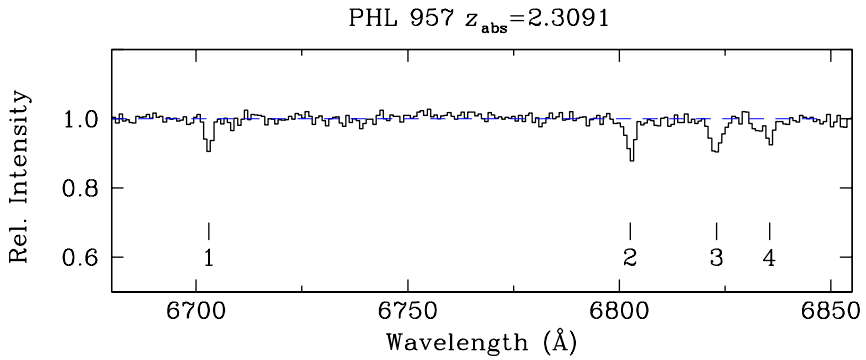

FIGURE 6. Portion of the Palomar spectrum of the bright QSO PHL 957 recorded by Pettini et al. (1990), encompassing the region of the Zn II and Cr II absorption lines in the $z_{\rm abs} = 2.3091$ DLA. The vertical tick marks indicate the positions of the lines as follows. Line 1: Zn II λ2025.483; line 2: Cr II λ2055.596; line 3: Cr II λ2061.575 + Zn II λ2062.005 (blended); and line 4: Cr II λ2065.501. The spectrum has been normalised to the underlying QSO continuum and is shown on an expanded vertical scale.

solid form in the interstellar media traced by DLAs and, by inference, be an indication of the presence of dust in these early galaxies (Cr is also singly ionised in H I gas).

From the point of view of chemical evolution, both Zn and Cr closely trace Fe in Galactic stars with metallicities [Fe/H] between 0 (i.e. solar) and -2 (1/100 of solar; Sneden, Gratton, & Crocker 1991, McWilliam et al. 1995). Additional advantages are the convenient rest wavelengths of the Zn II and Cr II transitions, which at $z = 2 - 3$ (where DLAs are most numerous in current samples) are redshifted into a easily observed portion of the optical spectrum, and the inherently weak nature of these lines which ensures that they are nearly always on the linear part of the curve of growth, where column densities can be derived with confidence from the measured equivalent widths (e.g. Bechtold 2002).

All in all, a small portion of the red spectrum of a QSO with a damped Lyα system has the potential of providing some important chemical clues on the nature of these absorbers and the evolutionary status of the population of galaxies they trace. One of the first detections of Zn and Cr in a DLA is reproduced in Figure 6. However, data of sufficiently high signal-to-noise ratio to detect the weak absorption lines of interest (or to place interesting upper limits on their equivalent widths) typically require nearly one night of observation per QSO with a 4 m class telescope. Consequently, it was necessary to wait until the mid-1990s before a sufficiently large sample of Zn and Cr measurements in DLAs could be assembled.

Figure 7 shows the current data set from the survey by our group (e.g. Pettini et al. 1997b; 1999). There are several interesting conclusions which can be drawn from these results.

(*a*) Damped Lyα systems are generally metal poor at all redshifts sampled. Evidently DLAs arise in galaxies at early stages of chemical evolution, since nearly all of the points in Figure 7 lie below the line of solar abundance. The statistic of relevance here is the the column density-weighted mean abundance of Zn

$$[\langle {\rm Zn/H_{DLA}} \rangle] = \log\langle ({\rm Zn/H})_{\rm DLA} \rangle - \log\ ({\rm Zn/H})_{\odot}, \qquad (2.4)$$

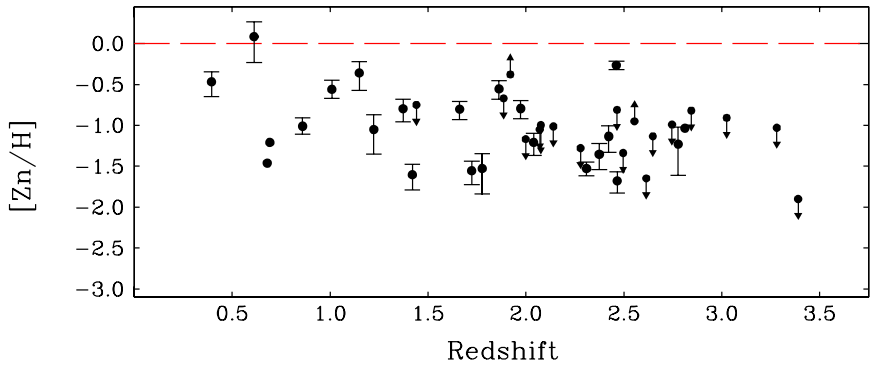

FIGURE 7. Plot of the abundance of Zn against redshift for the full sample of 41 DLAs from the surveys by Pettini and collaborators. Abundances are measured on a log scale relative to the solar value shown by the broken line at [Zn/H] = 0.0; thus a point at [Zn/H] = −1.0 corresponds to a metallicity of 1/10 of solar. Upper limits, corresponding to non-detections of the Zn II lines, are indicated by downward-pointing arrows. Upward-pointing arrows denote lower limits in two cases where the Zn II lines are sufficiently strong that saturation may be important.

where

$$\langle (\mathrm{Zn/H})_{\mathrm{DLA}} \rangle = \frac{\sum_{i=1}^{n} N(\mathrm{Zn\ II})_i}{\sum_{i=1}^{n} N(\mathrm{H\ I})_i}, \tag{2.5}$$

and the summations in eq. (2.5) are over the n DLA systems in a given sample. In this way, by counting all the Zn atoms per unit cross-section (cm^{-2}) and dividing by the total column density of neutral hydrogen we find that DLAs have a typical metallicity of only $\sim 1/13$ of solar ($[\langle \mathrm{Zn/H_{DLA}} \rangle] = -1.13$).

(*b*) There appears to be a large range in the values of metallicity reached by different galaxies at the same redshift. Values of [Zn/H] in Figure 7 span nearly two orders of magnitude, pointing to a protracted 'epoch of galaxy formation' and to the fact that chemical enrichment probably proceeded at different rates in different DLAs. The wide dispersion in metallicity goes hand in hand with the diverse morphology of the DLA galaxies which have been imaged at $z < 1$, as discussed earlier (§2.1).

When the metallicity distribution of damped Lyα systems is compared with those of different stellar populations of the Milky Way, we find that is broader and peaks at lower metallicities than those of either thin or thick disk stars (Figure 8). At the time when our Galaxy's metal enrichment was at levels typical of DLAs, its kinematics were closer to those of the halo and bulge than a rotationally supported disk. This finding is at odds with the proposal that most DLAs are large disks with rotation velocities in excess of 200 km s^{-1}, put forward by Prochaska & Wolfe (1998).

(*c*) There is little evidence from the data in Figure 7 for any redshift evolution in the metallicity of DLAs. This question has also been addressed using the abundance of Fe which, thanks to its rich absorption spectrum, can be followed to higher redshifts and lower metallicities than Zn (Prochaska, Gawiser, & Wolfe 2001). Once allowance is made for the fraction of Fe in dust grains, Vladilo (2002b) finds a gradient of −0.32 in the linear regression of [Fe/H] vs. z_{abs}. However, while Figure 7 suggests that the chances of finding a DLA with [Zn/H] > -1.0 are possibly greater at $z < 1$, the column density-

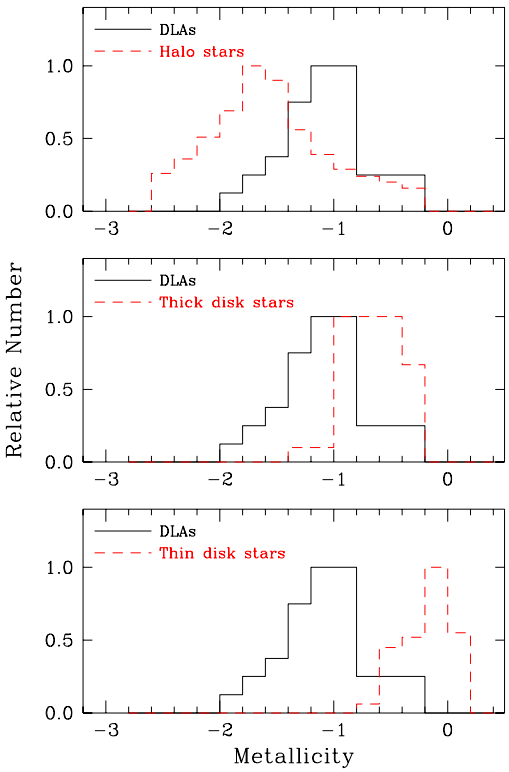

FIGURE 8. Metallicity distributions, normalised to unity, of DLAs at $z \simeq 2-3$ and of stars belonging to the disk (Wyse & Gilmore 1995) and halo (Laird et al. 1988) populations in the Milky Way.

weighted metallicities—which measure the density of metals per comoving volume—are consistent with no evolution over the range of redshifts probed so far, irrespectively of whether Zn or Fe are considered (see Figure 9). Evidently, the census of metals at all redshifts is dominated by high column density systems of low metallicity.

The lack of evolution in both the neutral gas and metal content of DLAs was unexpected and calls into question the notion that these absorbers are unbiased tracers of these quantities on a global scale. On the other hand, the paucity of data at redshifts $z < 1$, that is over a time interval of more than half of the age of the universe (Table 1), makes it difficult to draw firm conclusions and it may yet be possible to reconcile existing measurements with models of cosmic chemical evolution (Pei, Fall, & Hauser 1999; Kulkarni & Fall 2002).

2.4. *Element Ratios*

So far we have considered only the overall metallicity of DLAs as measured by the [Zn/H] ratio. However, the relative abundances of different elements offer additional insights into the chemical evolution of this population of galaxies, as we shall now see. This aspect of the work has really blossomed with the advent of efficient echelle spectrographs on both

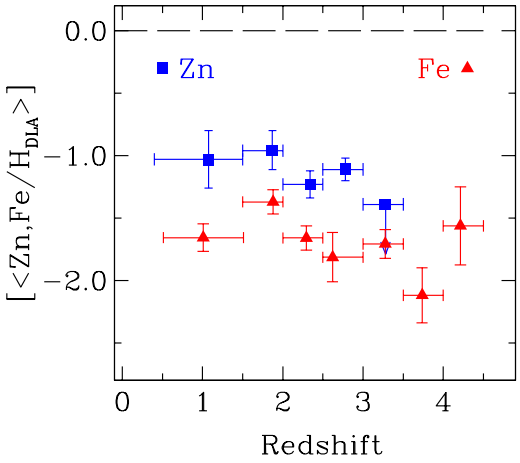

FIGURE 9. Column density-weighted metallicities of DLAs in different redshift intervals, from the surveys by Pettini et al. (1999) for Zn, and Prochaska & Wolfe (2002) for Fe. The lower abundance of Fe relative to Zn probably reflects the presence of moderate amounts of dust in most DLAs (Vladilo 2002b).

the Keck and VLT facilities, which have allowed the absorption lines of a wide variety of elements to be recorded simultaneously, often with exquisite precision.

2.4.1. *Dust in DLAs*

The presence of dust in DLAs can be inferred by comparing the gas phase abundances of two elements which in local interstellar clouds are depleted by differing amounts. The [Cr/Zn] ratio is one of the most suitable of such pairs for the reasons described above. It became apparent from the earliest abundance measurements in DLAs that this ratio is generally sub-solar, as expected if a fraction of the Cr has been incorporated into dust grains. Figure 10 shows this result for a subset of the DLAs in Figure 7; similar plots are now available for larger samples of DLAs and for other pairs of elements, one of which is refractory and the other is not (e.g. Prochaska & Wolfe 1999; 2002).

From this body of data it is now firmly established that the depletions of refractory elements are generally lower in DLAs than in interstellar clouds of similar column density in the disk of the Milky Way. The reasons for this are not entirely clear. The question has not yet been addressed quantitatively; qualitatively the effect is probably related to the lower metallicities of the DLAs and the likely higher temperature of the interstellar medium in these absorbers (Wolfire et al. 1995; Petitjean, Srianand, & Ledoux 2000; Kanekar & Chengalur 2001). Figure 10 does seem to indicate a weak trend of decreasing Cr depletion with decreasing metallicity, also supported by the results of Prochaska & Wolfe (2002).

Typically, it is found that refractory elements are depleted by about a factor of two in DLAs—a straightforward average of the measurements in Figure 10 yields a mean $\langle$[Cr/Zn]$\rangle = -0.3^{+0.15}_{-0.2}$ (1σ limits). When we combine this value with the mean metallicity of DLAs, $[\langle \mathrm{Zn/H_{DLA}} \rangle] = -1.13$, or $\langle Z_{\mathrm{DLA}} \rangle = 1/13\, Z_{\odot}$, we reach the conclusion that in damped systems the "typical" dust-to-gas ratio is only about $\approx 1/30$ of the Milky Way value (although there is likely to be a large dispersion from DLA to DLA, reflecting the range of metallicities evident in Figure 7). In the disk of our Galaxy, there a well determined relationship between the neutral hydrogen column density and the visual

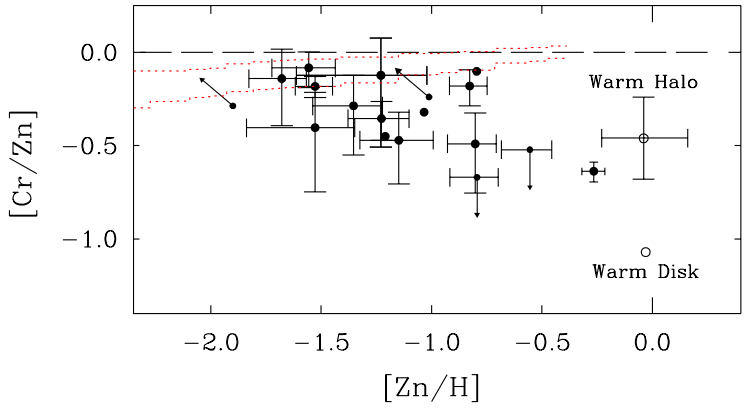

FIGURE 10. (Reproduced from Pettini et al. 1997a). Cr abundance relative to Zn in 18 damped Lyα systems (filled symbols). The region within the dotted lines (reproduced from Ryan, Norris, & Beers 1996) indicates how the [Cr/Fe] ratio varies in Galactic stars in this metallicity regime. The open circles show the typical [Cr/Zn] ratios measured in interstellar clouds in the disk and halo of our Galaxy, where the underabundance of Cr relative to Zn is ascribed to dust depletion (Savage & Senbach 1996).

extinction, $\langle N(\mathrm{H\ I})\rangle/\langle A_V\rangle = 1.5\times10^{21}$ cm^{-2} mag^{-1} (Diplas & Savage 1994), where A_V is the extinction (in magnitudes) in the V band. For the typical damped Lyα system with neutral hydrogen column density $N(\mathrm{H\ I}) = 1\times10^{21}$ cm^{-2} and dust-to-gas ratio 1/30 that of the local ISM, we therefore expect a trifling $A_V \simeq 0.02$ mag in the rest-frame V band. Of more interest is the far-UV extinction, since this is the spectral region observed at optical wavelengths at redshifts $z = 2-3$. Adopting the SMC extinction curve (Bouchet et al. 1985)—which may be the appropriate one to use at the low metallicities of most DLAs—we calculate that a damped Lyα system will typically introduce an extinction at 1500 Å of $A_{1500} \simeq 0.1$ mag in the spectrum of a background QSO. Such a small degree of obscuration is consistent with the mild reddening found in the spectra of QSO with DLAs, compared to the average UV continuum slope of QSOs without (Pei, Fall, & Bechtold 1991).

2.4.2. *Alpha-capture elements*

The moderate degree of depletion of refractory elements in DLAs has motivated a number of attempts to correct for the fractions missing from the gas phase (Vladilo 2002a and references therein) and thereby explore *intrinsic* (rather than dust-induced) departures from solar relative abundances. The basic idea, which is discussed extensively in the contribution to this volume by Francesca Matteucci, is that different elements are produced by stars of different masses and therefore different lifetimes. Thus, the relative abundances of two elements can, under the right circumstances, provide clues to the previous star formation history of the galaxy, or stellar population, under consideration (Wheeler, Sneden, & Truran 1989). Such clues are not always easy to decipher, however. For one thing, they rely on our incomplete, and mostly theoretical, knowledge of the stellar yields. Secondly, we must assume a 'standard' initial mass function (IMF) because, if we were free to alter at will the relative proportions of high and low mass stars, then we would obviously be able to reproduce most element ratios, but we could scarcely claim to have learnt anything in the process. Fortunately, all available evidence (including that

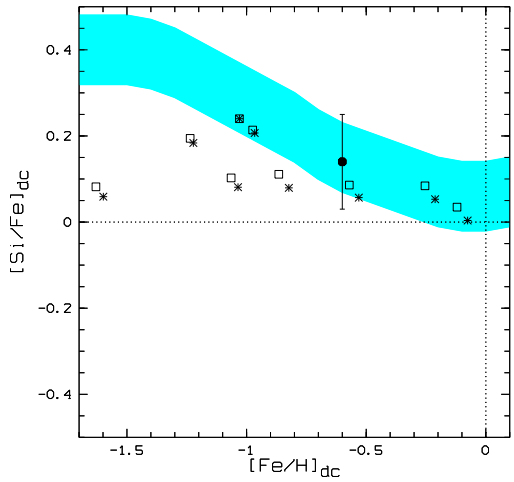

FIGURE 11. (Reproduced from Ledoux et al. 2002). Dust-corrected abundance ratios of Si relative to Fe versus DLA metallicity, as measured from the dust-corrected Fe abundances. Errors are typically ± 0.1 dex. Different symbols are used for different dust depletion patterns adopted when correcting the observed abundances. The shaded area shows the region occupied by Galactic stars in the disk and halo over this range of metallicities.

from DLAs, Molaro et al. 2001) points to a universal IMF as a reasonable first order approximation (Kennicutt 1998a).

One of the cornerstones of this kind of approach is the well established overabundance of the alpha-capture elements relative to Iron in metal-poor stars of the Galactic halo. Mg, Si, Ca, and Ti are generally overabundant by factors of between two and three in stars where Fe is below one tenth solar, i.e. $[\alpha/\mathrm{Fe}] = +0.3$ to $+0.5$ when $[\mathrm{Fe/H}] \lesssim -1.0$ (Ryan et al. 1996). This result can be understood if approximately two thirds of the Fe (and other Fe-peak) elements are produced by Type Ia supernovae (SN) and released into the ISM with a time lag of about 1 Gyr relative the α-capture elements (and one third of the Fe) manufactured by the massive stars which explode as Type II supernovae.

In this picture, 1 Gyr is therefore the time over which the halo of our Galaxy became enriched to a metallicity $[\mathrm{Fe/H}] = -1$, ultimately reflecting the rate at which star formation proceeded in this stellar component of the Milky Way. Clearly, the situation could be different in other environments (Gilmore & Wyse 1991; Matteucci & Recchi 2001). The thick disk, for example, evidently reached solar abundances of the α-elements in less than 1 Gyr, since the α overabundance—or more correctly the Fe deficiency—seems to persist to this high level of metallicity (Fuhrmann 1998).

Do damped Lyα systems, which as we have seen are generally metal-poor, show an overabundance of the α elements? This question has been addressed by several authors and there seems to be a general consensus that there is not a unique answer. As can be seen from Figure 11, while some DLAs conform to the pattern seen in Galactic stars, many others do not, in that they exhibit near solar values of [Si/Fe] even when [Fe/H] is $\ll -1$ (Molaro et al. 2000; Pettini et al. 2000a; Ledoux et al. 2002; Prochaska & Wolfe 2002; Vladilo 2002b). Presumably, these are galaxies where star formation has proceeded only slowly, or intermittently, allowing the Fe abundance to 'catch up' with that of the Type II supernova products. The Magellanic Clouds may be local counterparts of these DLAs (Pagel & Tautvaisiene 1998). Thus, the chemical clues provided by the these

element ratios are another demonstration, together with the wide range in metallicity at the same epoch (§2.3) and the morphologies of the absorbers (§2.1), that DLAs trace a diverse population of galaxies, with different evolutionary histories. Their common trait is simply a large cross-section on the sky at a high surface density of neutral hydrogen.

2.4.3. *The Nucleosynthesis of Nitrogen*

A case of special interest is Nitrogen, whose nucleosynthetic origin is a subject of considerable interest and discussion. There is general agreement that the main pathway is a six step process in the CN branch of the CNO cycle which takes place in the stellar H burning layer, with the net result that ^{14}N is synthesised from ^{12}C and ^{16}O. The continuing debate, however, centres on which range of stellar masses is responsible for the bulk of the nitrogen production. A comprehensive reappraisal of the problem was presented by Henry, Edmunds, & Köppen (2000) who compiled an extensive set of abundance measurements and computed chemical evolution models using published yields. Briefly, nitrogen has both a primary and a secondary component, depending on whether the seed carbon and oxygen are those manufactured by the star during helium burning, or were already present when the star first condensed out of the interstellar medium.

Observational evidence for this dual nature of nitrogen is provided mainly from measurements of the N and O abundances in H II regions. (For consistency with other published work, we depart here from the notation used throughout the rest of this article, and use parentheses to indicate logarithmic ratios of number densities; adopting the recent reappraisal of solar photospheric abundances by Holweger (2001), we have $(\mathrm{N/H})_\odot = -4.07$; $(\mathrm{O/H})_\odot = -3.26$; and $(\mathrm{N/O})_\odot = -0.81$). In H II regions of nearby galaxies, (N/O) exhibits a strong dependence on (O/H) when the latter is greater than $\sim 2/5$ solar; this is generally interpreted as the regime where secondary N becomes dominant. At low metallicities on the other hand, when (O/H) $\lesssim -4.0$ (that is, $\lesssim 1/5$ solar), N is mostly primary and tracks O; this results in a plateau at (N/O) $\simeq -1.5$ (see Figure 12).

The principal sources of primary N are thought to be intermediate mass stars, with masses $4 \lesssim M/M_\odot \lesssim 7$, during the asymptotic giant branch (AGB) phase. A corollary of this hypothesis is that the release of N into the ISM should lag behind that of O which, as we have seen, is widely believed to be produced by massive stars which explode as Type II supernovae soon after an episode of star formation. Henry et al. (2000) calculated this time delay to be approximately 250 Myr; at low metallicities the (N/O) ratio could then perhaps be used as a clock with which to measure the past rate of star formation, as proposed by Edmunds & Pagel (1978). Specifically, in metal-poor galaxies which have only recently experienced a burst of star formation one may expect to find values of (N/O) *below* the primary plateau at (N/O) $\simeq -1.5$, provided the fresh Oxygen has been mixed with the ISM (Larsen, Sommer-Larsen, & Pagel 2001).

As pointed out by Pettini, Lipman, & Hunstead (1995), clues to the nucleosynthetic origin of nitrogen can also be provided by measurements of N and O in high redshift DLAs. Apart from the obvious interest in taking such abundance measurements to the distant past, when galaxies were young, one of the advantages of DLAs is that, thanks to their generally low metallicities, they probe a regime where local H II region abundance measurements are sparse or non-existent and where the effect of a delayed production of primary nitrogen should be most pronounced.

Figure 12 shows the most recent compilation of data relevant to this question. The fact that all DLA measurements fall within the region in the (N/O) vs. (O/H) plot bounded by the primary and secondary levels of N production provides empirical evidence in support of currently favoured ideas for the nucleosynthesis of primary N by intermediate

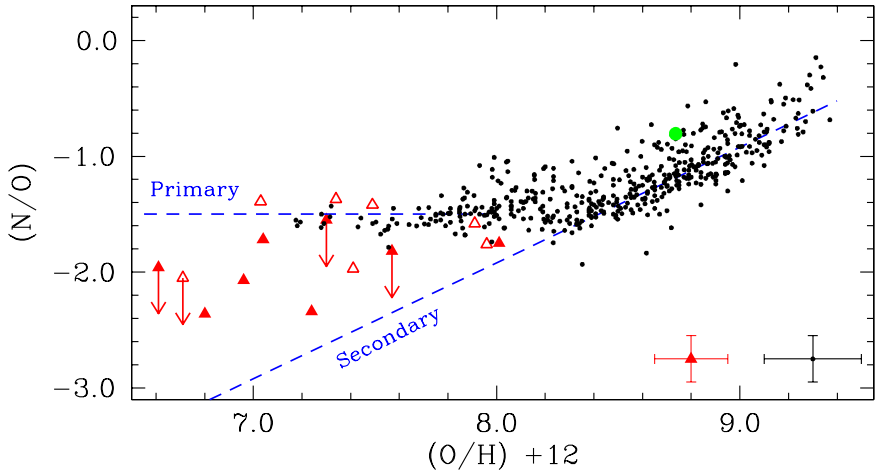

FIGURE 12. Abundances of N and O in extragalactic H II regions (small dots) and damped Lyα systems (large triangles). Sources for the H II region measurements are given in Pettini et al. (2002a). Filled triangles denote DLAs where the abundance of O could be measured directly, while open triangles are cases where S was used as a proxy for O. The error bars in the bottom right-hand corner give an indication of the typical uncertainties; the large dot corresponds to the solar abundances of N and O from the recent reappraisal by Holweger (2001). The dashed lines are approximate representations of the secondary and primary levels of N production (see text).

mass stars. The uniform value $(\mathrm{N/O}) \simeq -1.5$ seen in nearby metal-poor star-forming galaxies can be understood in this scenario if these galaxies are not young, but contain older stellar populations, as indicated by a number of imaging studies with *HST*.

It is also somewhat surprisingly to find such a high proportion (40%) of DLAs which have apparently not yet attained the full primary level of N enrichment at $(\mathrm{N/O}) \simeq -1.5$. Possibly, the low metallicity regime—where the difference between secondary and primary nitrogen enrichment is most pronounced—preferentially selects young galaxies which have only recently condensed out of the intergalactic medium and begun forming stars. A more speculative alternative, which needs to be explored computationally, is that at low metallicities stars with masses lower than $4M_{\odot}$ may make a significant contribution to the overall N yield (Lattanzio et al., in preparation; Meynet & Maeder 2002). The release of primary N may, under these circumstances, continue for longer than 250 Myr, perhaps for a substantial fraction of the Hubble time at the median $\langle z \rangle = 2.5$ of our sample.

In concluding this section, it is evident that DLAs are a rich source of information on nucleosynthesis in the early stages of galaxy formation. Element abundances in DLAs are increasingly being taken into consideration, together with stellar and H II region data from local systems, in models of the chemical evolution of galaxies and in the calculation of stellar yields. The chemical clues they provide will be even more valuable once their connection to today's galaxies in the Hubble sequence is clarified.

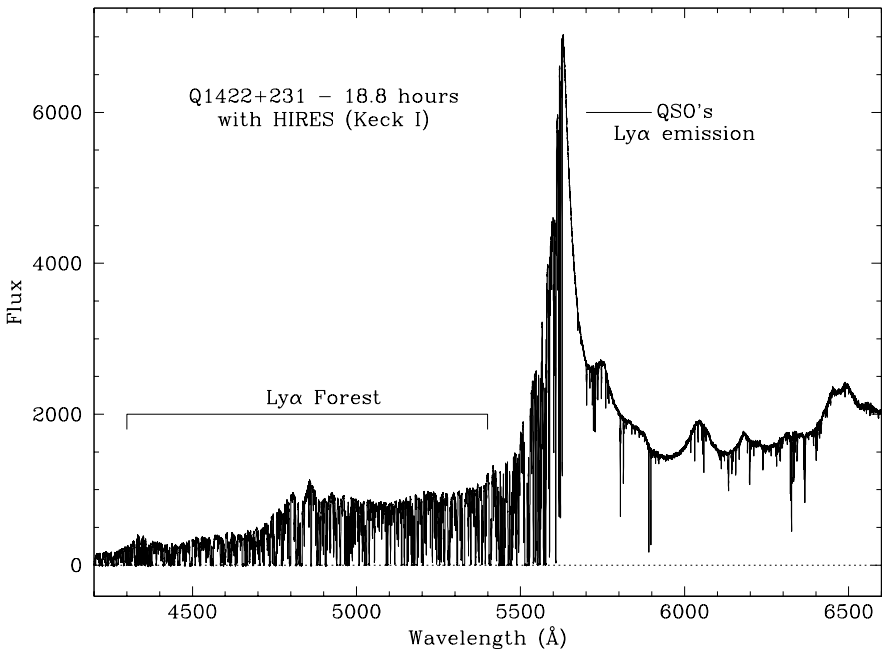

FIGURE 13. (Reproduced from Ellison 2000). This is one of the best QSO spectra ever obtained thanks to the combination of the bright magnitude of the gravitationally lensed QSO Q1422+231 ($V = 16.5$), long exposure time (amounting to several nights of observation), and high spectral resolution offered by the Keck echelle spectrograph (FWHM $\simeq 8\,\mathrm{km\ s^{-1}}$). The signal-to-noise ratio in the continuum longwards of the Lyα emission line is between 200 and 300. At these high redshifts ($z_{\rm em} = 3.625$) the Lyα forest eats very significantly into the QSO spectrum below the Lyα emission line and, with the present resolution, breaks into hundreds of absorption components (see Figure 14).

3. The Lyman Alpha Forest

The next component to be considered is the all-pervading intergalactic medium which manifests itself as a multitude of individual Lyα absorption lines bluewards of the Lyα emission line of every QSO. As can be appreciated from Figures 13 and 14, the effect is dramatic at high redshift. Observationally, the term Lyα forest is used to indicate absorption lines with column densities in the range $10^{16} \gtrsim N(\mathrm{HI}) \gtrsim 10^{12}$ cm^{-2} (see Figure 5).

Hydrodynamical simulations have shown that the Lyα forest is a natural consequence of the formation of large scale structure in a universe dominated by cold dark matter and bathed in a diffuse ionising background (see Weinberg, Katz, & Hernquist 1998 for an excellent review of the ideas which have led to this interpretation). An example is reproduced in Figure 15. Artificial spectra generated by throwing random sightlines through such model representations of the high redshift universe are a remarkably good match to real spectra of the Lyα forest. In particular, the simulations are very successful at reproducing the column density distribution of H I in Figure 5, the line widths and profiles, and the evolution of the line density with redshift. Consequently, much of what we have learnt about the IGM in the last few years has been the result of a very productive interplay between observations of increasing precision and simulations

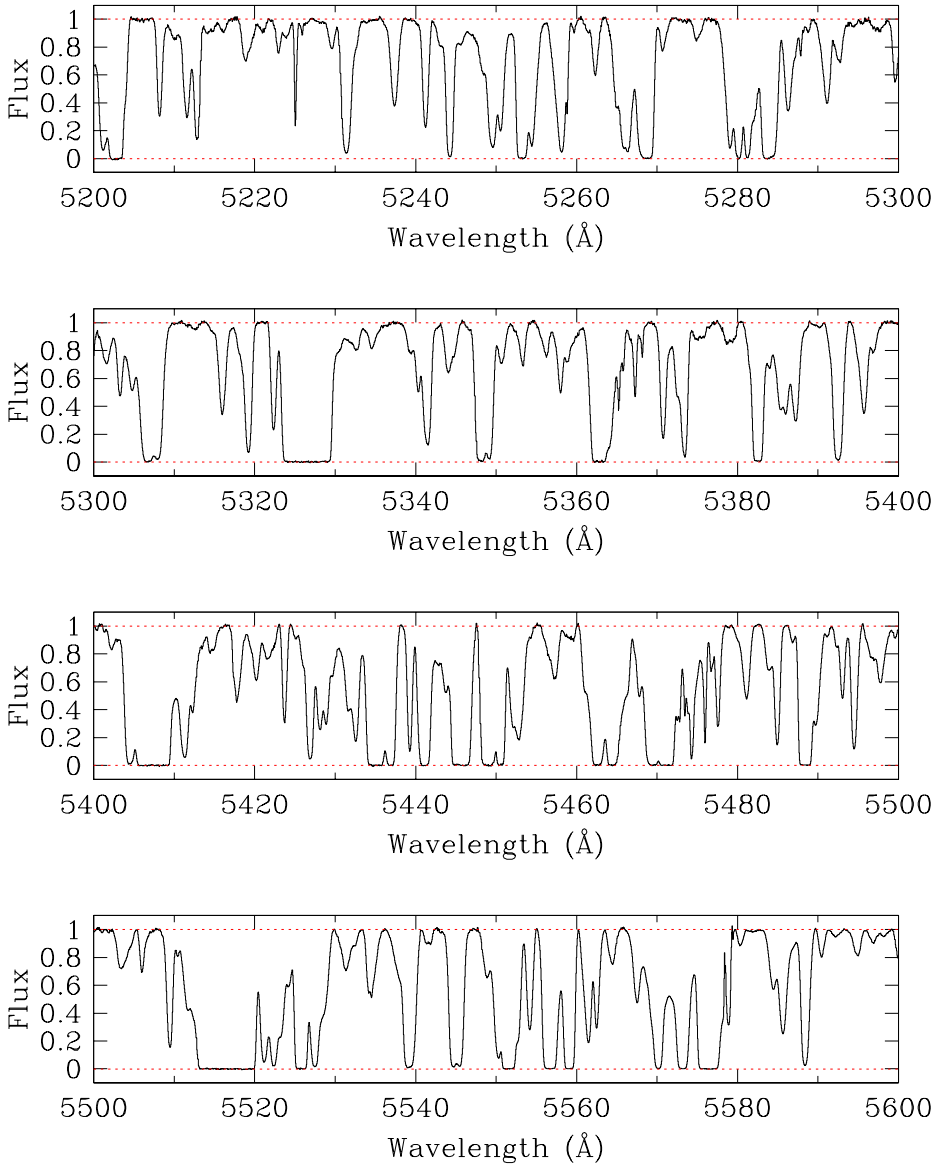

FIGURE 14. (Reproduced from Ellison 2000). Portion of the Lyα forest between $z_{\rm abs} = 3.277$ and 3.607 in the Keck spectrum of Q1422+231 shown in Figure 13. There are more than 50 individual absorption components in each 100 Å-wide stretch of spectrum.

of increasing sophistication. This modern view of the Lyα forest is often referred to as the 'fluctuating Gunn-Peterson' effect.

There are two important properties of the Lyα forest which we should keep in mind. One is that it is highly ionised, so that the H I we see directly is only a small fraction ($\sim 10^{-3}$ to $\sim 10^{-6}$) of the total amount of hydrogen present. With this large ionisation

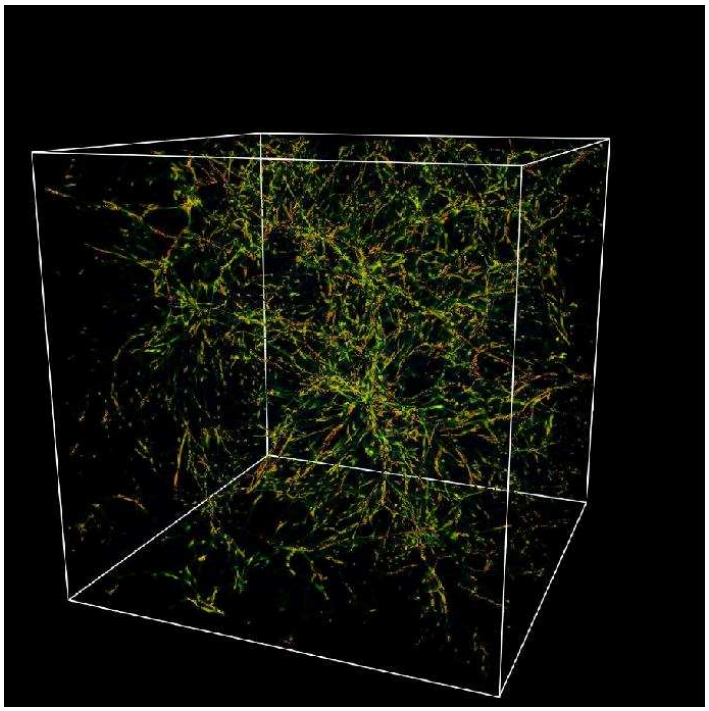

FIGURE 15. (Reproduced from http://astro.princeton.edu/~cen). Distribution of neutral gas at $z = 3$ from hydrodynamic cosmological simulation in a spatially flat, COBE-normalized, cold dark matter model with the cosmological parameters adopted in this article (§1.1). The box size is $25\,\mathrm{Mpc}/h$ (comoving) on the side, and the number of particles used in the simualation is 768^3. The structure seen in this (and other similar simulations) reproduces very well the spectral properties of the Lyα forest when artificial spectra are generated along random sightlines through the box.

correction it appears that the forest can account for most of the baryons at high, as well as low, redshift (Rauch 1998; Penton, Shull, & Stocke 2000); that is $\Omega_{\mathrm{Ly}\alpha} \approx 0.02\ h^{-2}$. Second, the physics of the absorbing gas is relatively simple and the run of optical depth $\tau(\mathrm{Ly}\alpha)$ with redshift can be thought of as a 'map' of the density structure of the IGM along a given line of sight. At low densities, where the temperature of the gas is determined by the balance between photoionisation heating (produced by the intergalactic ionising background) and adiabatic cooling (due to the expansion of the universe), $\tau(\mathrm{Ly}\alpha) \propto (1+\delta)^{1.5}$, where δ is the overdensity of baryons $\delta \equiv (\rho_{\mathrm{b}}/\langle\rho_{\mathrm{b}}\rangle - 1)$. At $z = 3$, $\tau(\mathrm{Ly}\alpha) = 1$ corresponds to a region of the IGM which is just above the average density of the universe at that time ($\delta \approx 0.6$). The last absorption line in the second panel of Figure 14, near 5395 Å, is an example of a Lyα line with $\tau \simeq 1$. The idea that, unlike galaxies, the forest is an unbiased tracer of mass has prompted, among other things, attempts to recover the initial spectrum of density fluctuations from consideration of the spectrum of line optical depths in the forest (Croft et al. 2002)

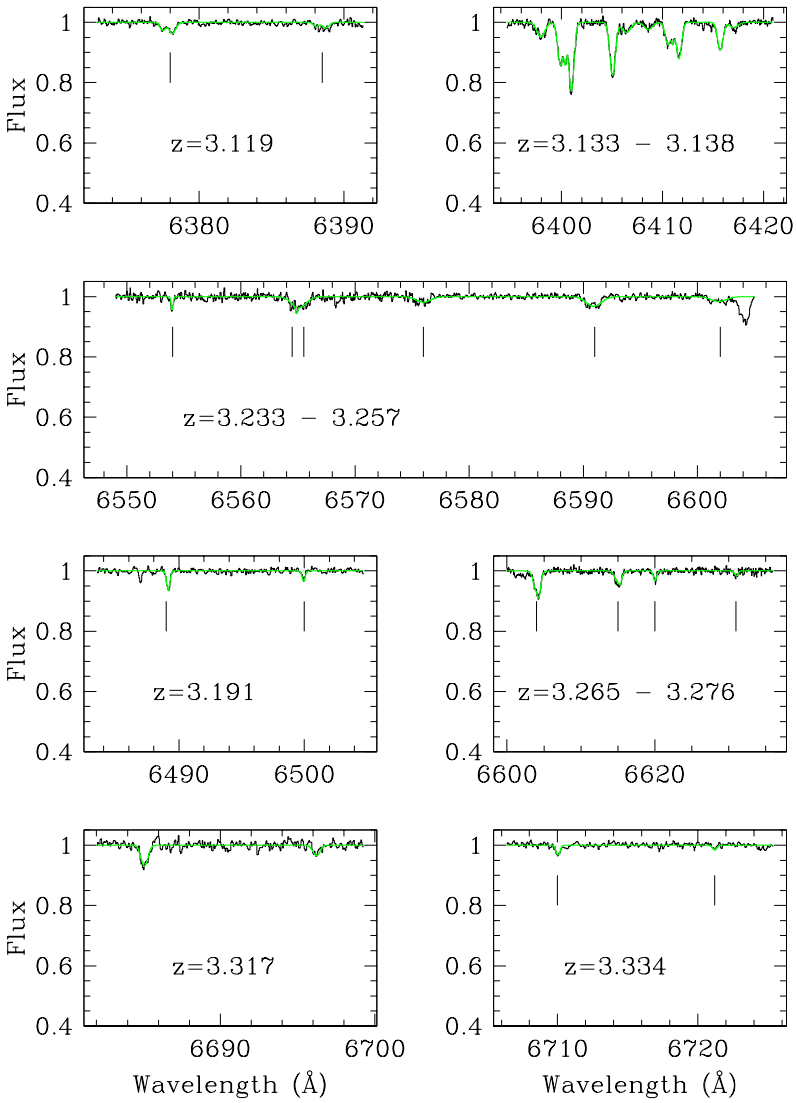

FIGURE 16. (Reproduced from Ellison et al. 2000). Examples of weak C IV lines identified in the spectrum of Q1422+231; most of these would have remained undetected in spectra of lower signal-to-noise ratios. Green (grey) lines show the profile fits used to deduce the column density of C IV. The weakest C IV systems are indicated with tick marks to guide the eye.

3.1. *Metals in the Lyα Forest*

The lack of associated metal lines was originally one of the defining characteristics of the Lyα forest and was interpreted as evidence for a primordial origin of the clouds (Sargent et al. 1980). However, this picture was shown to be an oversimplification by the first observations—using the HIRES spectrograph on the Keck I telescope—with sufficient sensitivity to detect the weak C IV $\lambda\lambda 1548, 1550$ doublet associated with Lyα clouds with column densities $\log N(\mathrm{H\ I}) \gtrsim 14.5$ (Cowie et al. 1995; Tytler et al. 1995). Typical

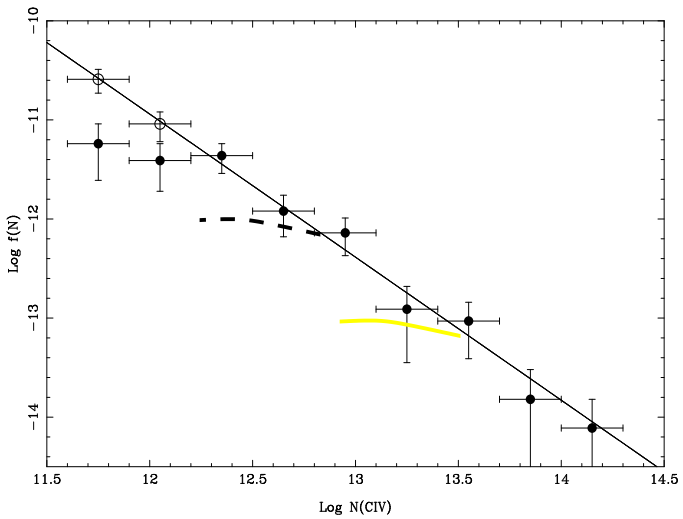

FIGURE 17. (Reproduced from Ellison 2000). C IV column density distribution in Q1422+231 at $\langle z \rangle = 3.15$; $f(N)$ is the number of C IV systems per column density interval and per unit redshift path. The filled circles are the data; the straight line shows the best fitting power-law slope $\alpha = 1.44$, assuming the distribution to be of the form $f(N)dN = BN^{-\alpha}dN$. The open circles show the values corrected for incompleteness at the low column density end; with these correction factors there is no indication of a turnover in the column density distribution down to the lowest values of N(C IV) reached up to now. Earlier indications of a turnover shown by the grey (Petitjean & Bergeron 1994) and dashed (Songaila 1997) curves are now seen to be due to the less sensitive detection limits of those studies, rather than to a real paucity of weak Lyα lines.

column density ratios in these clouds are $N(\text{C IV})/N(\text{H I}) \simeq 10^{-2}$ – 10^{-3}, indicative of a carbon abundance of about 1/300 of the solar value, or $[\text{C/H}] \simeq -2.5$ in the usual notation, and with a scatter of perhaps a factor of ~ 3 (Davé et al. 1998).

The question of interest is 'Where do these metals come from?'. Obviously from stars (we do not know of any other way to produce carbon!), but are these stars located in the vicinity of the Lyα clouds observed—which after all are still at the high column density end of the distribution of values of N(H I) for intergalactic absorption—or are we seeing a more widespread level of metal enrichment, perhaps associated with the formation of the first stars which re-ionised the universe at $z > 6$ (Songaila & Cowie 2002)?

To answer this question we should like to search for metals in low density regions of the IGM, away from the overdensities where galaxies form. Observationally, this is a very difficult task—the associated absorption lines, if present at all, would be very weak indeed. Ellison et al. (1999, 2000) made some progress towards probing such regions using extremely long exposures with HIRES of two of the brightest known high-z QSOs, both gravitationally lensed: APM 08279+5255 and Q1422+231. The latter set of data in particular (Figures 13 and 14) is of exceptionally high quality, reaching a signal-to-noise ratio S/N $\simeq 300$ which translates to a limiting rest-frame equivalent width limit $W_0(3\sigma) \leq 1$ mÅ; this in turn corresponds to a sensitivity to C IV absorbers with column densities as low as $N(\text{C IV}) \simeq 4 \times 10^{11}$ cm^{-2}.

And indeed C IV lines are found at these low levels (see Figure 16), showing that metals are present in the lowest column density Lyα clouds probed, at least down to $N(\text{H I}) = 10^{14}$ cm^{-2}. As can be seen from Figure 17, the number of weak C IV lines

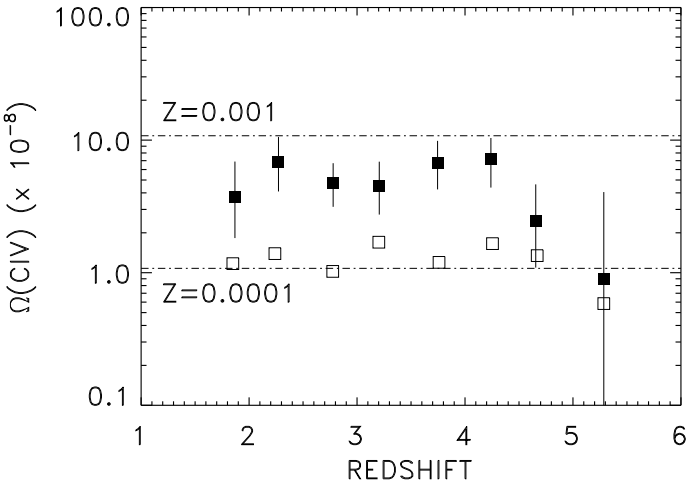

FIGURE 18. (Reproduced from Songaila 2001). Mass density in C IV (expressed as fraction of the closure density—see eqs. 2.2 and 2.3) as a function of redshift. The filled symbols are for C IV absorption systems in the range $12 \leq \log N(\mathrm{C\ IV}) \leq 15$ (cm^{-2}). The dot-dash lines show values of Ω(CIV) computed assuming $\Omega_b\, h^2 = 0.022, h = 0.65$, a C IV ionisation fraction of 0.5, and metallicities $Z = 0.0001$ and $0.001\, Z_\odot$, respectively.

continues to rise as the signal-to-noise ratio of the spectra increases and any levelling off in the column density distribution presumably occurs at $N(\mathrm{C\ IV}) < 5 \times 10^{11}$ cm^{-2}. This limit is one order of magnitude more sensitive than those reached previously. In other words, we have yet to find any evidence in the Lyα forest for regions of the IGM which are truly of primordial composition or have abundances as low as those of the most metal-poor stars in the Milky Way halo. These conclusions are further supported by the recent detection of O VI $\lambda\lambda$1032, 1038 absorption in the Lyα forest at $z = 2$ by Carswell, Schaye, & Kim (2002). In agreement with the results of Ellison et al. (2000), these authors found that most Lyα forest clouds with $N(\mathrm{H\ I}) \geq 10^{14}$ cm^{-2} have associated O VI absorption and that [O/H] is in the range -3 to -2. Weak O VI lines from regions of lower Lyα optical depth have not yet been detected directly, but their presence is inferred from statistical considerations (Schaye et al. 2000).

3.2. *C IV at the Highest Redshifts*

A level of metal enrichment of 10^{-3} to 10^{-2} of solar in regions of the IGM with $N(\mathrm{H\ I}) \geq 10^{14}$ cm^{-2} may still be understood in terms of supernova driven winds from galaxies. The work of Aguirre et al. (2001) shows that such outflows which, as we shall shortly see (§4.5) are observed directly in Lyman break galaxies at $z = 3$, may propagate out to radii of several hundred kpc before they stall. However, if O VI is also present in Lyα forest clouds of lower column density, as claimed by Schaye et al. (2000), an origin in pregalactic stars at much earlier epochs is probably required (Madau, Ferrara, & Rees 2001).

In order to investigate this possibility, Songaila (2001) extended the search for intergalactic C IV to $z = 5.5$, taking advantage of the large number of QSOs with $z_{\rm em} > 5$ discovered by the Sloan Digital Sky Survey. The surprising result, reproduced in Figure 18, is that there seems to be no discernable evolution in the integral of the column density distribution of C IV from $z = 1.5$ to $z = 5.5$. (The reality of a possible drop in Ω(CIV)

beyond $z = 4.5$ is questioned by Songaila because incompleteness effects have not been properly quantified in this difficult region of the optical spectrum, at $\lambda_{\rm obs} > 8500\,$Å). This finding was unexpected and has not yet been properly assessed. The observed column density of C IV depends not only on the overall abundance of Carbon, but also on the shape and normalisation of the ionising background and on the densities associated with a given N(H I). Thus, we would have predicted large changes in Ω(CIV) between $z = 5.5$ and 1.5 in response to the evolving density of ionising sources (QSOs) and the development of structure in the universe, even if the metallicity of the IGM had remained constant between these two epochs.

Whatever lies behind the apparent lack of redshift evolution of Ω(CIV), it is clear that the IGM was enriched with the products of stellar nucleosynthesis from the earliest times we have been able to probe with QSO absorption line spectroscopy, only $\sim 1\,$Gyr after the Big Bang. The measurements of Ω(CIV) in Figure 18 suggest a metallicity $Z_{\rm Ly\alpha} \gtrsim 10^{-3} Z_\odot$; this is a lower limit because it assumes that the ionisation of the gas is such that the ratio C IV/$\rm C_{tot}$ is near its maximum value of about 0.5. This minimum metallicity can in turn can be used to infer a minimum number of hydrogen ionising photons (with energy $h\nu \geq 13.6\,$eV, corresponding to $\lambda \leq 912\,$Å) in the IGM, because the progenitors of the supernovae which produce Oxygen, for example, are the same massive stars that emit most of the (stellar) ionising photons. Assuming a solar relative abundance scale (i.e. [C/O] = 0), Madau & Shull (1996) calculated that the energy of Lyman continuum photons emitted is 0.2% of the rest-mass energy of the heavy elements produced.† From this it follows that

$$\frac{N_{\rm photons}}{N_{\rm baryons}} \times 13.6\,{\rm eV} \simeq 0.002 m_{\rm p} c^2\, Z \simeq 2 \times 10^6\,{\rm eV} \times Z \qquad (3.6)$$

(Miralda-Escudé & Rees 1997), where Z is the metallicity (by mass) and $m_{\rm p}$ the mass of the proton. Since $Z_\odot = 0.02$ (Grevesse & Sauval 1998), if the Lyα forest at $z \simeq 5$ had already been enriched to a metallicity $Z_{\rm Ly\alpha} \simeq 10^{-3}\, Z_\odot$, eq. (3.6) implies that by that epoch stars had emitted approximately three Lyman continuum (LyC) photons per baryon in the universe. Whether this photon production is sufficient to have reionised the IGM by these redshifts depends critically on the unknown escape fraction of LyC photons from the sites of star formation.

4. Lyman Break Galaxies

Returning to Figure 1, it must be remembered that everything we have learnt on the distant universe up to this point required 'decoding' the information 'encrypted' in the absorption spectra of QSOs. It is easy to appreciate, therefore, the strong incentive which motivated astronomers in the 1990s to detect high resdshift galaxies directly. After many years of fruitless searches, we have witnessed since 1995 a veritable explosion of data from the *Hubble Deep Fields* and ground-based surveys with large telescopes. The turning point was the realisation of the effectiveness of the Lyman break technique (Figure 19) in preselecting candidate $z \simeq 3$ galaxies (Steidel et al. 1996). Although these galaxies constitute only $\sim 3 - 4\%$ of the thousands of faint objects, at all redshifts, revealed by a moderately deep CCD exposure at the prime focus of a 4 m telescope (see Figure 20), they can be readily distinguished on the basis of their colours alone, when observed through appropriately selected filters (Figure 21).

The Lyman break technique has been very successful at finding high redshift galaxies

† This is a lower limit if [C/O] < 0, as is the case for low metallicity gas in nearby galaxies (e.g. Garnett et al. 1999).

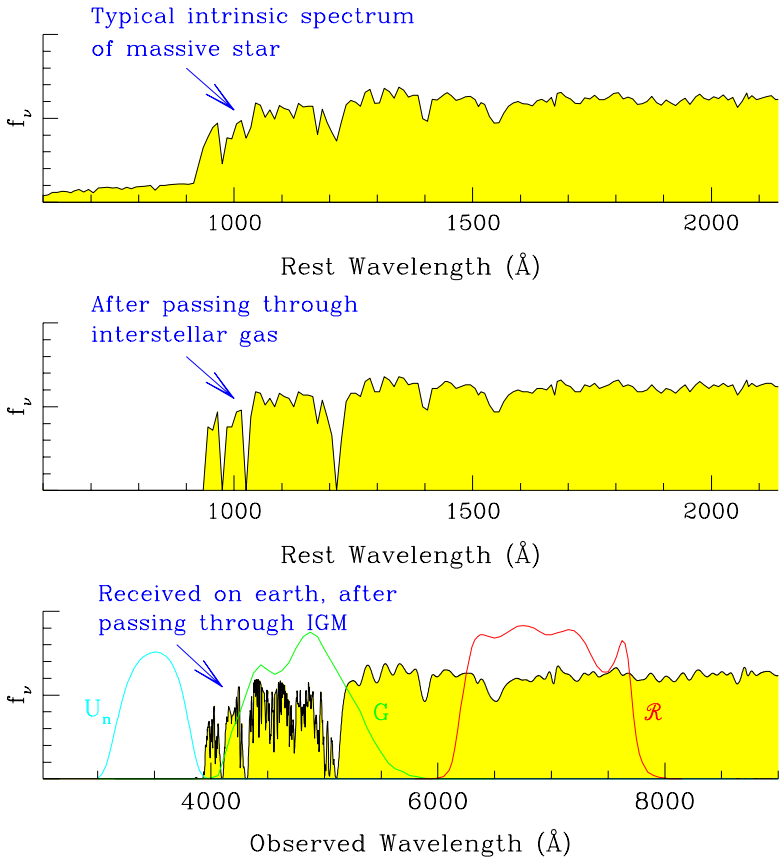

FIGURE 19. (Courtesy of Kurt Adelberger). An illustration of the principles behind the Lyman break technique. Hot stars have flat far-UV continua, but emit fewer photons below 912 Å, the limit of the Lyman series of hydrogen (top panel). These photons are also efficiently absorbed by any H I associated with the sites of star formation (middle panel) and have a short mean free path—typically only ~ 40 Å—in the IGM at $z = 3$. Consequently, when observed from Earth (bottom panel), the spectrum of a star forming galaxy at $z \simeq 3$ exhibits a marked 'break' near 4000 Å. With appropriately chosen broad-band filters, this spectral discontinuity gives rise to characteristic colours; objects at these redshifts appear blue in $(G - \mathcal{R})$ and red in $(U_n - G)$. For this reason, such galaxies are sometimes referred to as U-dropouts. A more quantitative description of the Lyman break technique can be found in Steidel, Pettini, & Hamilton (1995).

thanks to the combination of the increasingly large and UV sensitive CCDs used to identify candidates on the one hand, and the multi-object spectroscopic capabilities of large telescopes required for follow-up and confirmation on the other. Thus, samples of spectroscopically confirmed $z \simeq 3$ galaxies have grown from zero to more than one thousand in the space of only five years. As can be seen from Figure 22, the spectroscopic redshifts generally conform to expectations based on just two colours. Such large samples have made it possible to trace the star formation history of the universe over most of the Hubble time and to measure the large-scale properties of this population of galaxies, most notably their clustering and luminosity functions (see Steidel 2000 for a review).

In parallel with this work on the Lyman break population as a whole, in the last few

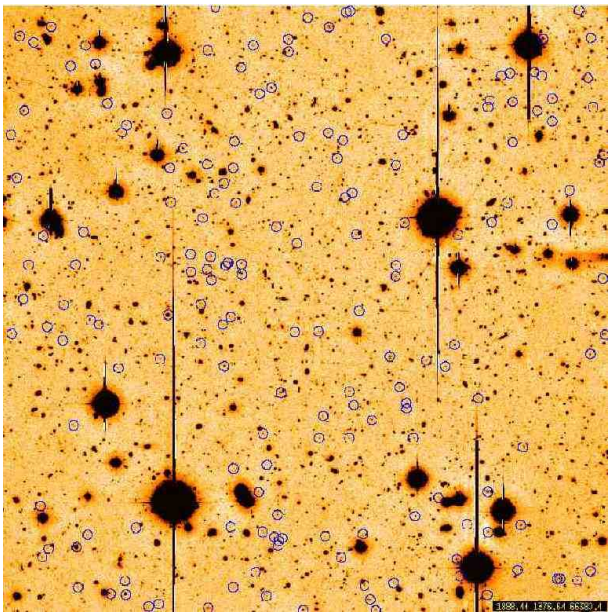

FIGURE 20. A typical deep CCD image recorded at the prime focus of a 4m-class telescope. This particular image (of the field designated DSF2237b) was obtained with the COSMIC camera of the Palomar Hale telescope, by exposing for a total of two hours through a custom made $\mathcal{R}$ filter. In the 9×9 arcmin field of view (corresponding to co-moving linear dimensions of $11.6 \times 11.6\, h^{-1}$ Mpc at $z = 3$) there are ~ 3300 galaxies brighter than $\mathcal{R} = 25.5$; 140 of these (circled) show Lyman breaks which place them at redshifts between $z = 2.6$ and 3.4 .

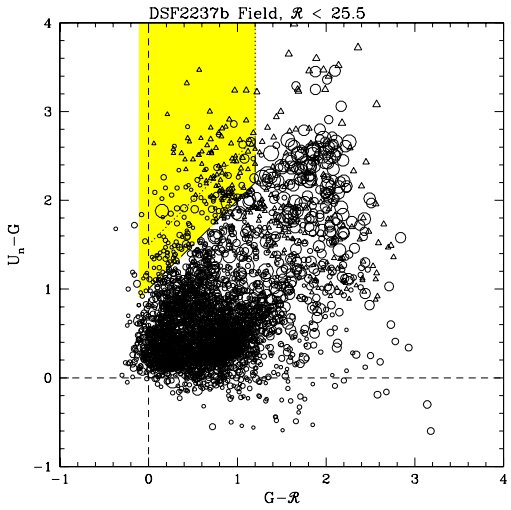

FIGURE 21. All the ~ 3300 galaxies from Figure 20 are included in this colour–colour plot. The shaded region shows how the 140 candidate Lyman break galaxies are selected for subsequent spectroscopic follow-up. The symbol size is proportional to the object magnitude; circles denote objects detected in all three bands, while triangles are lower limits in $(U_n - G)$ for U_n dropouts.

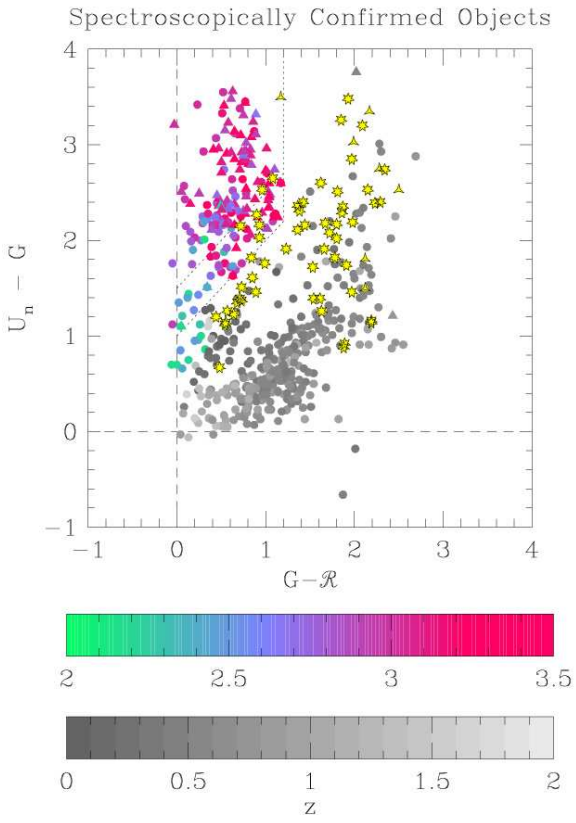

FIGURE 22. The location of spectroscopically confirmed galaxies (from the surveys by Steidel and collaborators) on the $(U_n - G)$ vs. $(G - \mathcal{R})$ plot. Triangles denote objects undetected in the U_n band; stellar symbols are used for Galactic stars.

years we have also begun to study in more detail the physical properties of some of the brighter galaxies in the sample. The questions which we would like to address are:

(*a*) What are the stellar populations of the Lyman break galaxies?

(*b*) What are their ages and masses?

(*c*) What are their levels of metal enrichment?

(*d*) What are the effects of star formation at high z on the galaxies and the surrounding IGM?

Many of these questions link observational cosmology with stellar and interstellar astrophysics, and this will become evident as we now explore them in turn.

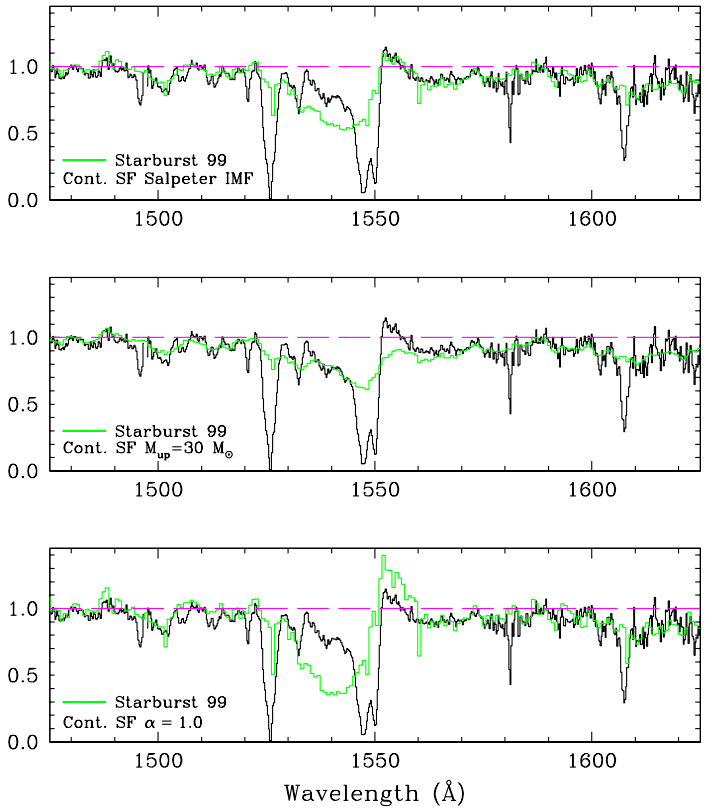

FIGURE 23. Comparisons between *Starburst99* (Leitherer et al. 1999) population synthesis models with different IMFs (green lines) and the Keck spectrum of MS 1512-cB58 analysed by Pettini et al. (2000b) in the region near the C IV doublet (black histogram). The y-axis is residual intensity.

4.1. *Stellar Populations and the Initial Mass Function*

Among the thousand or so known Lyman break galaxies (LBGs), one, designated MS 1512−cB58 (or cB58 for short) has provided data of exceptional quality, thanks to its gravitationally lensed nature. Discovered by Yee et al. (1996), cB58 is, as far as we can tell, a typical $\sim L^*$ galaxy at a redshift $z = 2.7276$ magnified by a factor of ~ 30 by the foreground cluster MS 1512+36 at $z = 0.37$ (Seitz et al. 1998). This fortuitous alignment makes it by far the brightest known member of the LBG population and has motivated a number of studies from mm to X-ray wavelengths.

When we record the spectrum of a $z = 3$ galaxy at optical wavelengths, we are in fact observing the redshifted far-UV light produced by a whole population of O and early B stars. Such spectra are most effectively analysed with population synthesis models, the most sophisticated of which is *Starburst99* developed by the Baltimore group (Leitherer et al. 1999). In Figure 23 we compare *Starburst99* model predictions for different IMFs with a portion of the moderate resolution Keck LRIS spectrum of cB58 obtained by Pettini et al. (2000b), encompassing the C IV $\lambda\lambda 1548, 1550$ doublet.

It is important to realise that the comparison only refers to *stellar* spectral features and does not include the *interstellar* lines, readily recognisable by their narrower widths

(the interstellar lines are much stronger in cB58, where we sample the whole ISM of the galaxy, than in the models which are based on libraries of nearby Galactic O and B stars). With this clarification, it is evident from Figure 23 that the spectral properties of at least this Lyman break galaxy are remarkably similar to those of present-day starbursts—a continuous star formation model with a Salpeter IMF provides a very good fit to the observations. In particular, the P-Cygni profiles of C IV, Si IV and N V are sensitive to the slope and upper mass limit of the IMF; the best fit in cB58 is obtained with a standard Salpeter IMF with slope $\alpha = 2.35$ and $M_{\rm up} = 100 M_\odot$ (top panel of Figure 23). IMFs either lacking in the most massive stars or, conversely, top-heavy seem to be excluded by the data (middle and bottom panels of Figure 23 respectively).

The only significant difference between the observed and synthesised spectra is in the optical depth of the P-Cygni absorption trough which is lower than predicted (top panel of Figure 23). A possible explanation is that this is an abundance effect—the strengths of the wind lines are known to be sensitive to the metallicity of the stars, since it is through absorption and scattering of photons in the metal lines that momentum is transferred to the gas and a wind is generated. The *Starburst99* spectra shown in Figure 23 are for solar metallicity, but a recent update (Leitherer et al. 2001) now includes stellar libraries compiled with *HST* observations of hot stars in the Large and Small Magellanic Clouds, taken to be representative of a metallicity $Z \simeq 1/3 Z_\odot$.

When these are compared with a higher resolution spectrum of cB58, obtained with the new Echelle Spectrograph and Imager (ESI) on the Keck II telescope, the match to the observed spectrum is improved (Figure 24). The emission component of the P-Cygni profile is perhaps underestimated by the model, but we suspect that there may be additional nebular C IV emission from the H II regions in the galaxy, superposed on the broader stellar P-Cygni emission. We take the good agreement in Figure 24 as an indication that the young stellar population of cB58 has reached a metallicity comparable to that of the Magellanic Clouds. This conclusion is reinforced by measurements of element abundances in the interstellar gas, as we shall see in §4.2 below.

Before leaving this topic, it is worth noting that with a modest amount of effort (and luck in the form of gravitational lensing) it is now possible to obtain spectra of high redshift galaxies of sufficient quality to distinguish between the OB stellar populations of the Milky Way and of the Magellanic Clouds. As a matter of fact, it is evident from Figure 24 that the resolution of the ESI spectrum of cB58 is superior to those of Magellanic Cloud stars (and of nearby starburst galaxies) with which we would like to compare it!

4.2. *Element Abundances in the Interstellar Gas*

The ESI spectrum of cB58, which covers the wavelength region from 1075 to 2800 Å at a resolution of 58 km s^{-1}, is a real treasure trove of information on this galaxy. For example, it includes 48 interstellar absorption lines of elements from H to Zn in a variety of ionisation stages, from neutral (H I, C I, O I, N I) to highly ionised species (Si IV, C IV, N V). The lines are fully resolved so that column densities can be derived from the analysis of their profiles. From these data Pettini et al. (2002b) were able to piece together for the first time a comprehensive picture of the chemical composition of the interstellar gas in a Lyman break galaxy (Figure 25) and examine the clues it provides on its evolutionary status and past history of star formation.

As can be seen from Figure 25, the ambient interstellar medium of cB58 is highly enriched in the elements released by Type II supernovae; O, Mg, Si, P, and S all have abundances of $\sim 2/5$ solar. Thus, even at this relatively early epoch ($z = 2.7276$ cor-

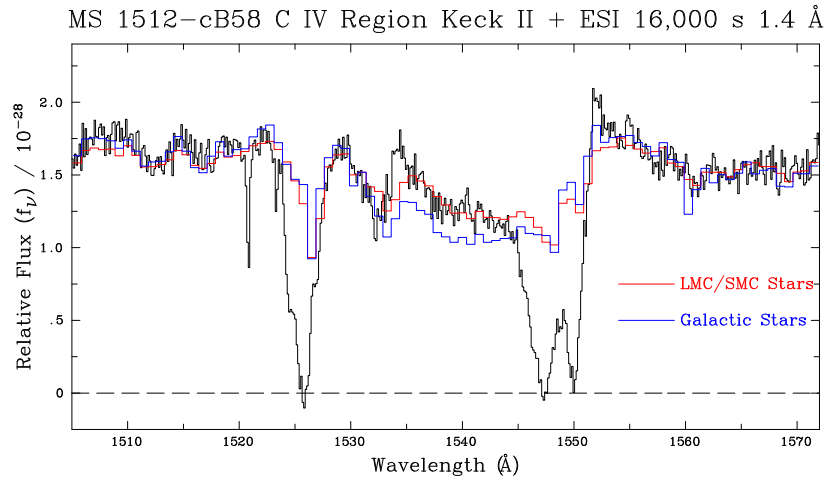

FIGURE 24. A portion of the high resolution spectrum of MS 1512-cB58 obtained by Pettini et al. (2002b), encompassing the C IV $\lambda\lambda 1548, 1550$ doublet lines, is compared with *Starburst99* synthetic spectra for solar and $\sim 1/3$ solar (LMC/SMC) metallicities (Leitherer et al. 2001).

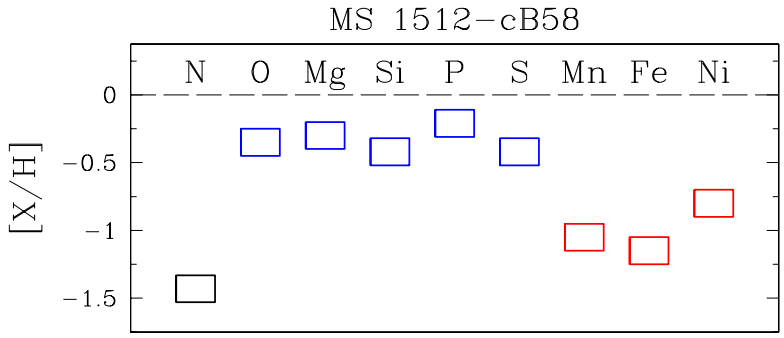

FIGURE 25. Pattern of chemical abundances in the ambient interstellar medium of cB58 deduced by Pettini et al. (2002b). The vertical height of the boxes shows the typical uncertainty in the abundance determinations. Blue boxes denote elements thought to be synthesised by massive stars which explode as Type II supernovae, while red boxes are for the Fe-peak elements predominantly produced by Type Ia SN. Their release into the ISM, as well as that of N from intermediate mass stars, lags behind that of the Type II SN products by several 100 Myr.

responds to 2.5 Gyr after the Big Bang in our adopted cosmology—see Table 1), this galaxy had already processed more than one third of its gas into stars.

Furthermore, cB58 appears to be chemically young, in that it is relatively deficient in elements produced by stars of intermediate and low mass with longer lifetimes than those of Type II SN progenitors. N and the Fe-peak elements we observe (Mn, Fe, and Ni) are all less abundant than expected by factors of between 0.4 and 0.75 dex. Depletion onto dust, which is known to be present in cB58, probably accounts for some of the Fe-peak element underabundances, but this is not likely to be an important effect for N. On the basis of current ideas of the nucleosynthesis of N, discussed in §2.4.3, it would appear that much of the ISM enrichment in cB58 has taken place within the last

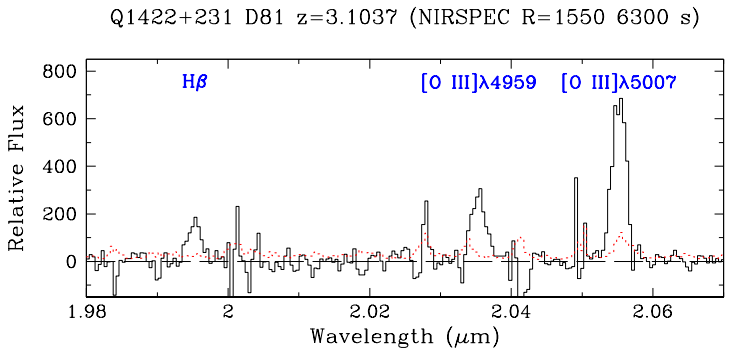

FIGURE 26. Example of a NIRSPEC K-band spectrum of a Lyman break galaxy from the survey by Pettini et al. (2001). The objects targeted typically have $K = 21$ (on the Vega scale) and remain undetected in the continuum. However, the nebular emission lines of [O III] $\lambda\lambda$4859, 5007, [O II] 3727 (not shown), and Hβ usually show up clearly with exposure times of 2–3 hours. The dotted line is the 1σ error spectrum.

250 Myr, the lifetime of the intermediate mass stars believed to be the main source of N. For comparison, the starburst episode responsible for the UV and optical light we see is estimated to be younger than ~ 35 Myr, on the basis of theoretical models of the spectral energy distribution at these wavelengths (Ellingson et al. 1996).

Taken together, these two findings are highly suggestive of a galaxy caught in the act of converting its interstellar medium into stars on a few dynamical timescales—quite possibly in cB58 we are witnessing the formation of a galactic bulge or an elliptical galaxy. The results of the chemical analysis are consistent with the scenario proposed by Shapley et al. (2001), whereby galaxies whose UV spectra are dominated by strong, blueshifted absorption lines, as is the case here, are the youngest in the range of ages of LBGs. These findings also lend support to models of structure formation which predict that, even at $z \simeq 3$, near-solar metallicities should in fact be common in galaxies with masses greater than $\sim 10^{10} M_\odot$ (e.g. Nagamine et al. 2001). The baryonic mass of cB58 is deduced to be $m_{\rm baryons} \simeq 1 \times 10^{10} M_\odot$, from consideration of its star formation history, metallicity, and the velocity dispersion of its ionised gas.

4.3. *The Oxygen Abundance in H II Regions*

How typical are these results of the Lyman break galaxy population as a whole? In the nearby universe, element abundances in star forming regions have traditionally been measured from the ratios of optical emission lines from H II regions. At $z = 3$ these features move to near-infrared (IR) wavelengths and have only become accessible in the last two years with the commissioning of high resolution spectrographs on the VLT (ISAAC) and Keck telescopes (NIRSPEC). Using these facilities, our group has recently completed the first spectroscopic survey of Lyman break galaxies in the near-IR, bringing together data for 19 LBGs; the galaxies are drawn from the bright end of the luminosity function, from $\sim L^*$ to $\sim 4\,L^*$ (Pettini et al. 2001). Figure 26 shows an example of the quality of spectra which can be secured with a 2–3 hour integration. In five cases we attempted to deduce values of the abundance of oxygen by applying the familiar $R_{23} = ([\mathrm{O\ II}] + [\mathrm{O\ III}])/\mathrm{H}\beta$ method first proposed by Pagel et al. (1979). We found that generally there remains a significant uncertainty, by up to 1 dex, in the value of (O/H) because of the double-valued nature of the R_{23} calibrator (see Figure 27).

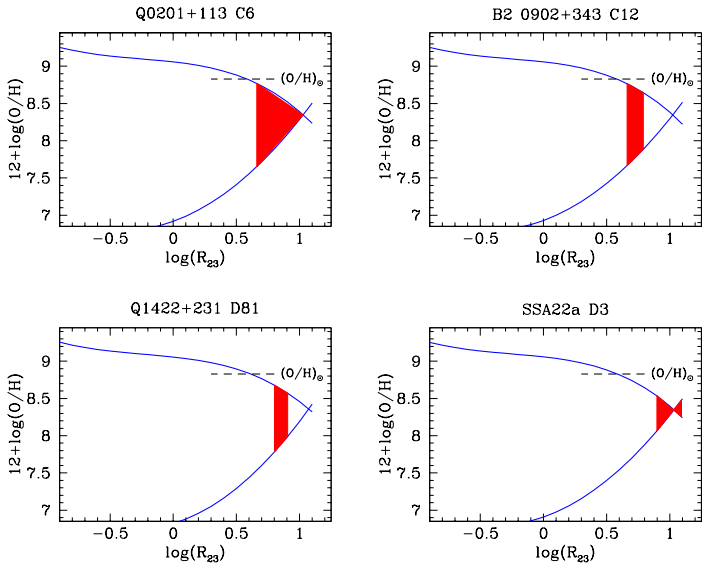

FIGURE 27. Oxygen abundance from the $R_{23} = ([\mathrm{O\ II}]+[\mathrm{O\ III}])/\mathrm{H}\beta$ ratio. In each panel the continuous lines are the calibration by McGaugh (1991) for the ionisation index $O_{32} = [\mathrm{O\ III}]/[\mathrm{O\ II}]$ appropriate to that object. The shaded area shows the values allowed by the measured R_{23} and its statistical 1σ error. The broken horizontal line gives for reference the solar abundance $12 + \log(\mathrm{O/H}) = 8.83$ from the compilation by Grevesse & Sauval (1998); the recent revision by Holweger (2001) would bring the line down by 0.09 dex.

Thus, in the galaxies observed, oxygen could be as abundant as in the interstellar medium near the Sun or as low as $\sim 1/10$ solar. When the R_{23} method is applied to cB58, a similar ambiguity obtains (Teplitz et al. 2000). The results from the analysis of the interstellar absorption lines described above (§4.2) resolve the issue by showing that the upper branch solution is favoured (we have no reason to suspect that the neutral and ionised ISM have widely different abundances). It remains to be established whether this is also the case for other LBGs.

In the near future this work will shift to lower and more easily accessible redshifts near $z = 2.2$ where all the lines of interest, from [O II] λ3727 to Hα, fall in near-IR atmospheric transmission windows. Nevertheless, the determination of element abundances from nebular emission lines will remain a time consuming task until multi-object spectrographs operating at near-IR wavelengths become available on large telescopes, or until the launch of the *Next Generation Space Telescope* (Kennicutt 1998b).

4.4. *Dating the Star Formation Activity*

Realistically, the detailed spectroscopic analysis described above can only be applied to a subset of LBGs, at the bright end of the luminosity funtion. However, the coarser spectral energy distribution (SED) of Lyman break galaxies still holds important information on the star formation episodes. Broad-band photometry in the optical and near-infrared, spanning the wavelength interval 900–5500 Å in the rest-frame, is now available for more than one hundred galaxies at $z \simeq 3$ (Papovich, Dickinson, & Ferguson 2001; Shapley et al. 2001). The colours over this range (typically four colours are used in the analysis) depend on the degree of dust reddening, $E(B-V)$, and on the age of the stellar population, t_{sf}. The two can be decoupled with some degree of confidence provided that the SED

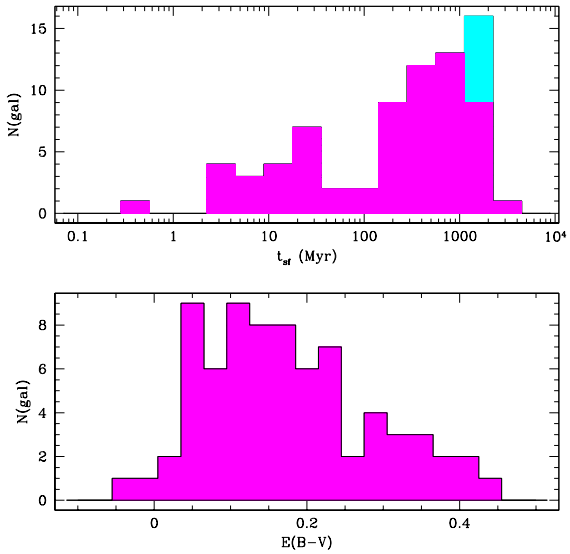

FIGURE 28. Histograms of best-fitting ages and reddening for the sample of 81 $z \simeq 3$ LBGs analysed by Shapley et al. (2001). There is a large spread of ages in the population; the median age is 320 Myr and 20% of the objects are older than 1 Gyr. The cyan (light grey) bin corresponds to galaxies with inferred ages older than the age of the universe at their redshifts (an indication of the approximate nature of the ages derived by SED fitting). The median $E(B-V) = 0.155$ for the sample corresponds to attenuations by factors of ~ 4.5 and ~ 2 at 1600 Å and 5500 Å respectively.

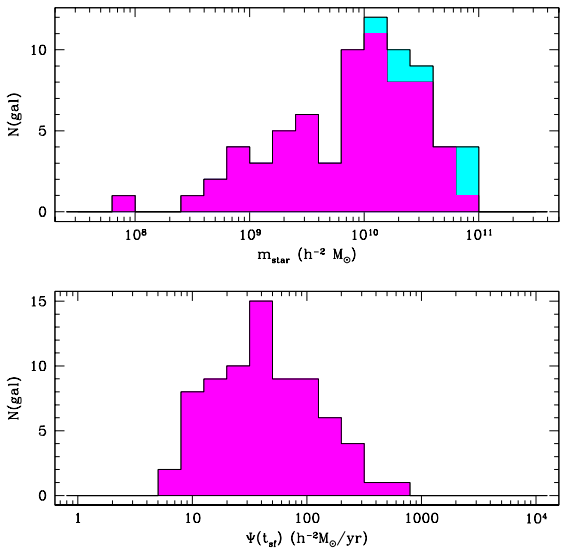

FIGURE 29. Histograms of assembled stellar mass and star formation rates from Shapley et al. (2001). By redshift $z \simeq 3$ a significant fraction of LBGs seem to be approaching the stellar mass of today's L^* galaxies, $m_{\rm star} \simeq 4 \times 10^{10} M_\odot$.

includes the age-sensitive Balmer break near 3650 Å, which at $z = 3$ falls between the H and K bands—hence the need for accurate near-IR photometry. A third parameter, the instantaneous star formation rate, $\Psi(t_{\rm sf})$, determines the normalisation (rather than the shape) of the SED. The analyses by Papovich et al. (2001) and Shapley et al. (2001) deduced the best-fitting values of $E(B-V)$, $t_{\rm sf}$, and $\Psi(t_{\rm sf})$ by χ^2 minimisation of the differences between the observed SEDs and those predicted by the widely used population synthesis code of Bruzual & Charlot (1993 and subsequent updates). The results have turned out to be very interesting—some would say surprising (see Figures 28 and 29).

Evidently, Lyman break galaxies span a wide range of ages. One fifth of the sample considered by Shapley et al. (2001) consists of objects which apparently have just collapsed and are forming stars on a dynamical timescale ($\sim 35\,$Myr). As we have seen, cB58 seems to belong to this class. At the other end of the scale, some 20% of the galaxies at $z = 3$ have been forming stars for more than 1 Gyr, placing the onset of star formation at much higher redshifts ($z > 5 - 10$). Furthermore, there appears to be a correlation between age and star formation rate, with the younger objects typically forming stars at about ten times the rate of the older ones and being more reddened on average. The mean SFR is $\langle\Psi(t_{\rm sf})\rangle = 210h^{-2}\,M_\odot$ yr^{-1} for galaxies with $t_{\rm sf} < 35\,$Myr while, for the 20% of the sample with $t_{\rm sf} > 1\,$Gyr, $\langle\Psi(t_{\rm sf})\rangle = 25h^{-2}\,M_\odot$ yr^{-1}.

This range of properties is further reflected in the total formed stellar masses $m_{\rm star}$ obtained by integrating $\Psi(t_{\rm sf})$ over $t_{\rm sf}$. A variety of star formation histories was considered (e.g. star formation which is continuous or decreases with time); in general $m_{\rm star}$ does not depend sensitively on this choice, although an older population of stars which by $z \simeq 3$ have faded at UV and optical wavelengths could remain hidden (Papovich et al. 2001). As can be seen from Figure 29, by redshift $z \simeq 3$ some galaxies had apparently already assembled a stellar mass comparable to that of an L^* galaxy today, $m_{\rm star} \simeq 4 \times 10^{10} M_\odot$, while 20% of the sample have values of $m_{\rm star}$ one order of magnitude smaller. These findings led Shapley et al. (2001) to speculate that we may be beginning to discern an evolutionary sequence in Lyman break galaxies, with the younger, dustier, more actively star-forming objects evolving to the older, less reddened, and more quiescent phase. It remains to be seen how this scenario stands up to the scrutiny of future observations, as we try to link the properties of the stellar populations of *individual* galaxies to other parameters, such as dynamical mass and metallicity.

4.5. *Galactic-Scale Outflows*

The near-IR spectroscopic survey by Pettini et al. (2001) confirmed a trend which had already been suspected on the basis of the optical (rest-frame UV) data alone. When the redshifts of the interstellar absorption lines, of the nebular emission lines, and of the resonantly scattered Lyα emission line are compared within the same galaxy, a systematic pattern of velocity differences emerges in all LBGs observed up to now (see Figure 30). We interpret this effect as indicative of galaxy-wide outflows, presumably driven by the supernova activity associated with the star-formation episodes. Such 'superwinds' appear to be a common characteristic of galaxies with large rates of star formation per unit area at high, as well as low, redshifts (e.g. Heckman 2001). They involve comparable amounts of matter to that being turned into stars (the mass outflow rate is of the same order as the star formation rate) and about 10% of the total kinetic energy delivered by the starburst (Pettini et al. 2000b). These outflows have a number of important astrophysical consequences.

First, they provide self-regulation to the star formation process—this is the 'feedback' required by theorists (e.g. Efstathiou 2000; Binney, Gerhard, & Silk 2001) for realistic

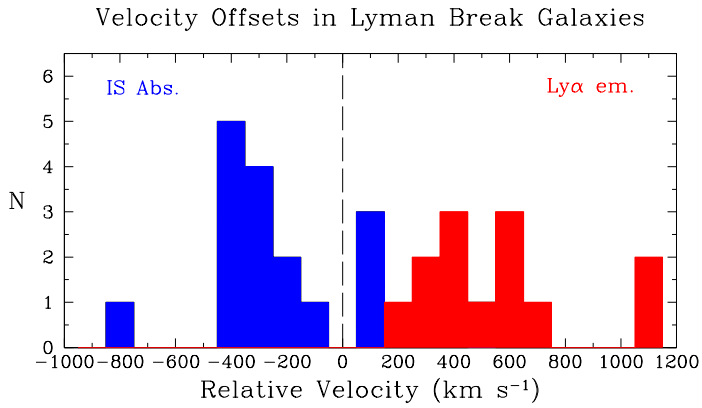

FIGURE 30. Velocity offsets of the interstellar absorption lines (blue or dark grey) and of the Lyα emission line (red or light grey) relative to [O III] and Hβ. Large scale motions of the order of several hundred km s^{-1} are indicated by the systematic tendency for the former to be blueshifted and the latter redshifted relative to the nebular emission lines.

galaxy formation models. Galactic winds may well be the key factor at the root of the 'evolutionary sequence' for LBGs just discussed (§4.4).

Second, they can distribute the products of stellar nucleosynthesis over large volumes of the intergalactic medium since the outflow speeds are likely to exceed the escape velocities in many cases. As we have seen, many LBGs are already metal-enriched at $z = 3$ and have by then been forming stars for much of the Hubble time. There is therefore at least the potential for widespread pollution of the IGM with metals, thereby explaining at least in part the results on the metallicity of the Lyα forest described in §3.1 and 3.2).

Third, the outflowing hot gas is likely to 'punch' through the neutral interstellar medium of the galaxies and provide a route through which Lyman continuum photons can leak out of the galaxies, easing the problem of how the universe came to be reionised (Steidel, Pettini, & Adelberger 2001). Indeed it now appears (Adelberger et al. 2002, in preparation) that LBGs have a substantial impact on the surrounding IGM, and that shock-ionisation by their winds leads to a pronounced 'proximity effect'—the Lyα forest is essentially cleared out by these outflows over radii of $\sim 100h^{-1}$ kpc.

5. Bringing it All Together

5.1. *A Global View of Metal Enrichment in the Universe Two Billion Years after the Big Bang*

We could briefly summarise everything we have covered so far as follows.

(*a*) The intergalactic medium at $z = 3$ does not consist entirely of pristine material. At least the regions we have been able to probe so far show traces of metals at levels between 1/1000 and 1/100 of solar metallicity. Matter in these regions, however, is still at a higher density than the mean density of the universe at that epoch, and it is unclear at present whether a pre-galactic episode of star formation (often referred to as Population III stars), is required to explain the large scale distribution of elements in the IGM.

(*b*) Damped Lyα systems have abundances similar to those of Population II stars in our Galaxy. Perhaps they represent an early stage in the formation of spiral galaxies, before most of the gas had been converted into stars. It is also clear that a wide variety

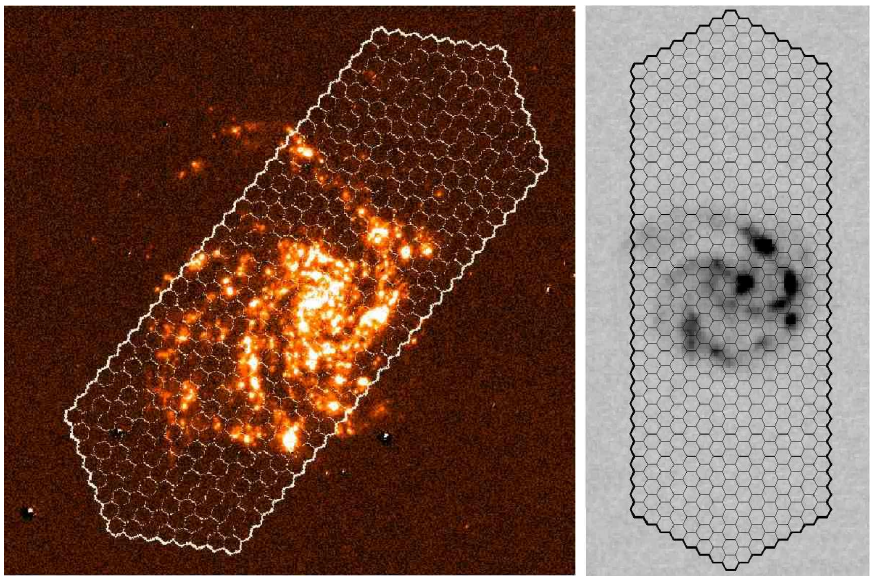

FIGURE 31. (Reproduced from Bunker et al. 2001). *Left:* An Hα image of the local spiral galaxy NGC 4254 as it would appear at $z = 1.44$ with the CIRPASS integral field unit overlaid (using 0.25 arcsec diameter fibres). *Right:* A spiral galaxy at $z \approx 1$ from the Hubble Deep Field B-band. The star-forming H II regions are prominent in the rest-frame UV. CIRPASS will accurately determine the true star formation rates, since (1) the compact knots of star formation are well-matched to the fibre size, reducing the sky background and increasing the sensitivity; (2) the large area surveyed by the integral field unit covers most of a spiral disk and (3) the Hα line is a much more robust measure of the star formation rate than the dust-suppressed UV continuum and resonantly-scattered Lyα.

of galaxy morphologies, including low surface brightness galaxies, share the common characteristic of providing a large cross-section on the sky at high surface densities of H I.

(c) Finally, Lyman break galaxies strongly resemble what we call Population I stars in the Milky Way. They are the sites of vigorous star formation which (i) has produced a relatively high level of chemical enrichment at early epochs, (ii) has built up stellar masses of $\gtrsim 10^{10}\,M_\odot$ in a sizeable fraction of the population, and (iii) drives large-scale outflows of gas, metals and dust into the intergalactic medium. All of these characteristics point to LBGs as the progenitors of today's spiral bulges and elliptical galaxies, observed during the most active phase in their lifetimes.

Table 2. Typical parameters of LBGs and DLAs at $z \simeq 3$

Property	LBGs	DLAs
SFR ($M_\odot$ yr^{-1})	~ 50	< 10
Z ($Z_\odot$)	$\sim 1/3$	$\sim 1/20$
Δv (km s^{-1})	~ 500	$\lesssim 200$

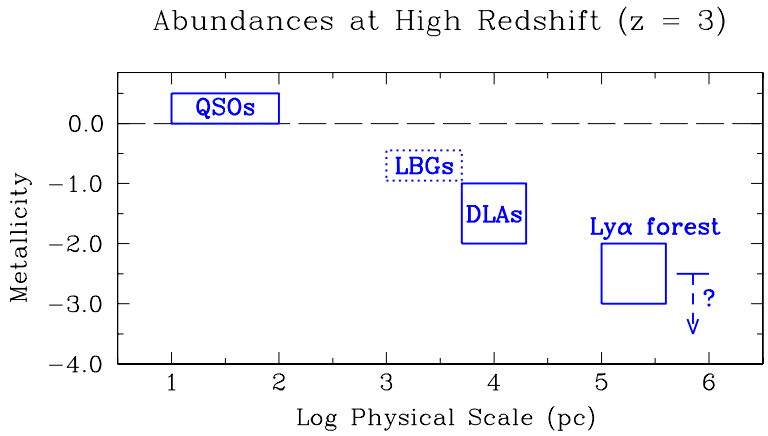

FIGURE 32. Summary of our current knowledge of abundances at high redshift. The 'metallicity' is plotted on the y-axis on a log scale relative to the solar reference; the latter is shown as the broken horizontal line at 0.0 and corresponds to approximately 2% of the baryons being incorporated in elements heavier than helium. The x-axis shows the typical linear dimensions of the strucures to which the abundance measurements refer, from the central regions of active galactic nuclei on scales of 10–100 pc to the intergalactic medium traced by the Ly α forest on Mpc scales. Generally speaking, these typical linear scales are inversely proportional to the overdensities of the structures considered relative to the background.

The connection between LBGs and DLAs is currently the subject of considerable discussion, as astronomers try and piece together these different pieces of the puzzle describing the universe at $z = 3$. Table 2 summarises some of the relevant properties. Lyman break galaxies have systematically higher star formation rates and metallicities, and their interstellar media have been stirred to higher velocities, than is the case in most DLAs. These seemingly contrasting properties can perhaps be reconciled if the two classes of objects are in fact drawn from the same luminosity function of galaxies at $z = 3$. Since they are selected from magnitude limited samples, the LBGs are preferentially bright galaxies—the data in Table 2 refer to galaxies brighter than L^* which corresponds to $\mathcal{R} = 24.5$ (Adelberger & Steidel 2000). If, on the other hand, the H I absorption cross-section decreases only slowly with galaxy luminosity, as is the case at lower redshifts (Steidel, Dickinson, & Persson 1994), the DLA counts would naturally be dominated by the far more numerous galaxies at the steep ($\alpha = -1.6$) faint end of the luminosity function.

Such a picture finds theoretical support in the results of hydrodynamical simulations and semi-analytic models of galaxy formation (e.g. Nagamine et al. 2001; Mo, Mao, & White 1999). In the coming years it will be tested by deeper and more extensive searches for DLA galaxies, by comparing the clustering of LBGs and DLAs (Adelberger et al. 2002, in preparation), and by more reliable measurements of the star formation activity associated with DLAs. This last project is best tackled in the near-infrared, by targeting the Hα emission line with integral field—rather than slit—spectroscopy, as provided for example by the Cambridge Infrared Panoramic Survey Spectrograph (CIRPASS—see Figure 31).

When we combine the available abundance determinations for Lyman break galaxies, damped Lyα systems and the Lyα forest with those for the inner regions of active galactic nuclei (from analyses of the broad emission lines and outflowing gas in broad absorption line QSOs—see Hamann & Ferland 1999), a 'snapshot' of metal enrichment

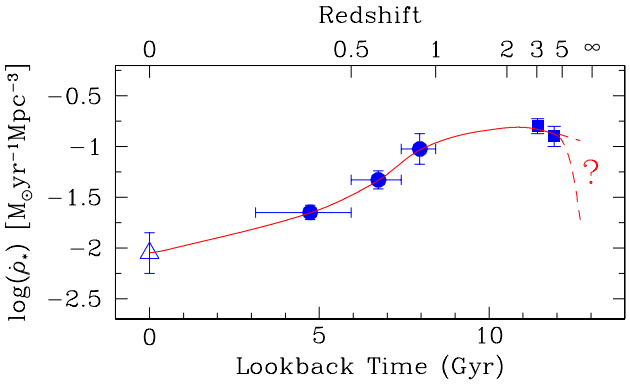

FIGURE 33. The comoving star formation rate density $\dot{\rho}_*$ vs. lookback time compiled from wide angle, ground based surveys (Steidel et al. 1999 and references therein). The data shown here are for a $H_0 = 50$ km s^{-1} Mpc^{-1}, $\Omega_{\rm M} = 1$, $\Omega_\Lambda = 0$ cosmology.

in the universe at $z \simeq 3$ emerges (Figure 32). The x-axis in the figure gives the typical linear dimensions of the structures to which the abundance measurements refer, from the 10–100 pc broad emission line region of QSOs, to the kpc scales of LBGs revealed by *HST* imaging (Giavalisco, Steidel, & Macchetto 1996), to the 10 kpc typical radii of DLAs deduced from their number density per unit redshift (Steidel 1993), to the 100 kpc dimensions of condensations in the Lyα forest with N(H I) $\gtrsim 10^{14}$ cm^{-2} indicated by the comparison of the absorption along adjacent sightlines in the real universe (e.g. Bechtold et al. 1994) and in the simulations (e.g. Hernquist et al. 1996).

These different physical scales in turn reflect the depths of the underlying potential wells and therefore the overdensities of matter in these structures relative to the mean density of the universe. Even from such an approximate sketch as Figure 32, it seems clear that it is this overdensity parameter which determines the degree of metal enrichment achieved at any particular cosmic epoch. Thus, even at the relatively early times which correspond to $z = 3$, the gas in the deepest potential wells where AGN are found had already undergone considerable processing and reached solar or super-solar abundances. At the other end of the scale, condensations in the Lyα forest which correspond to mild overdensities contained only traces of metals with metallicity $Z \simeq 1/100 - 1/1000\, Z_\odot$. The dependence of Z on the environment appears to be stronger than any age-metallicity relation—old does not necessarily mean metal-poor, not only for our own Galaxy but also on a global scale. This empirical conclusion can be understood in a general way within the framework of hierarchical structure formation in cold dark matter models (e.g. Cen & Ostriker 1999; Nagamine et al. 2001).

5.2. *Missing Metals?*

It can also be appreciated from Figure 32 that our knowledge of element abundances at high redshift is still very patchy. This becomes all the more evident when we attempt a simple counting exercise. Figure 33 shows a recent version of a plot first constructed by Madau et al. (1996) which attempts to trace the 'cosmic star formation history' by following the redshift evolution of the comoving luminosity density of star forming galaxies. This kind of plot enjoyed great popularity after it was presented by Madau et al.; more recently astronomers have approached it with greater caution as they have become more aware of the uncertainties involved. In particular, the dust corrections to

the data in Figure 33 have been the subject of intense debate over the last five years, as has been the contribution to $\dot{\rho}_*$ from galaxies which may be obscured at visible and ultraviolet wavelengths and only detectable in the sub-mm regime with instruments such as SCUBA. Furthermore, the normalisation of the plot depends on the IMF and on the slope of the faint end of the galaxy luminosity function. Nevertheless, if we assume that we have the story about right, some interesting consequences follow.

The first question one may ask is: *"What is the total mass in stars obtained by integrating under the curve in Figure 33?"* The data points in Figure 33 were derived assuming a Salpeter IMF (with slope -2.35) between $M = 100\ M_\odot$ and $0.1\ M_\odot$. However, for a more realistic IMF which flattens below $1\ M_\odot$, the values of $\dot{\rho}_*$ in Figure 33 should be reduced by a factor of 2.5.† With this correction:

$$\int_0^{13\ Gyr} \dot{\rho}_*'\ dt \simeq 3.3 \times 10^8\ M_\odot\ \mathrm{Mpc}^{-3} = 0.0043\ \rho_{\rm crit} \approx \Omega_{\rm stars}\ \rho_{\rm crit} \qquad (5.7)$$

where $\rho_{\rm crit} = 3.1 \times 10^{11}\, h^2\, M_\odot\, \mathrm{Mpc}^{-3}$ and $\Omega_{\rm stars} \simeq (1.5 - 3)\, h^{-1} \times 10^{-3}$ (Cole et al. 2001) is the fraction of the closure density contributed by stars at $z = 0$. Thus, within the rough accuracy with which this accounting can be done, the star formation history depicted in Figure 33 is apparently sufficient to produce the entire stellar content, in disks and spheroids, of the present day universe. Note also that $\approx 1/4$ of today's stars were made before $z = 2.5$ (the uncertain extrapolation of $\dot{\rho}_*$ beyond $z = 4$ makes little difference).

We can also ask: *"What is the total mass of metals produced by $z = 2.5$?"*. Using the conversion factor $\dot{\rho}_{\rm metals} = 1/42\ \dot{\rho}_*$ to relate the comoving density of synthesised metals to the star formation rate density (Madau et al. 1996) we find

$$\int_{11\ Gyr}^{13\ Gyr} \dot{\rho}_{\rm metals}\ dt \simeq 4.5 \times 10^6\ M_\odot\ \mathrm{Mpc}^{-3} \qquad (5.8)$$

which corresponds to

$$\Omega_Z \simeq 0.035 \times (\Omega_{\rm baryons} \times 0.0189) \qquad (5.9)$$

where $\Omega_{\rm baryons} = 0.088$ for $h = 0.5$ (§1.1) and 0.0189 is the mass fraction of elements heavier than helium for solar metallicity (Grevesse & Sauval 1998). In other words, the amount of metals produced by the star formation we *see* at high redshift (albeit corrected for dust extinction) is sufficient to enrich the whole baryonic content of the universe at $z = 2.5$ to $\approx 1/30$ of solar metallicity. Note that this conclusion does not depend sensitively on the IMF.

As can be seen from Table 3, this leaves us with a serious 'missing metals' problem which has also been discussed in more detail by Pagel (2002). The metallicity of damped Lyα systems is in the right ballpark, but $\Omega_{\rm DLA}$ is only a small fraction of $\Omega_{\rm baryons}$. Conversely, while the Lyα forest may account for a large fraction of the baryons, its metal content is one order of magnitude too low. The contribution of Lyman break galaxies to the cosmic inventory of metals is even more uncertain. The value in Table 3 is a strict (and not very informative) lower limit, calculated from the luminosity function of Steidel et al. (1999), taking into account *only* galaxies brighter than L^* and assigning to each a mass $M^* = 10^{11}\ M_\odot$ (which is likely to be a lower limit, as discussed by Pettini et al. 2001) and metallicity $Z = 1/3\ Z_\odot$. Galaxies fainter than L^* are not included in

† I have not applied this correction directly to Figure 33 in order to ease the comparison with earlier versions of this plot.

TABLE 3
CENSUS OF METALS AT $z = 2.5$[a]

Component	Ω[b]	Z[c]	Ω_Z[d]
Observed:			
DLAs	0.0025	0.07	0.002
Lyα Forest	$0.05 - 0.08$	0.003	$0.002 - 0.003$
Lyman Break Galaxies	?	0.3	> 0.0002
Predicted:			
All Baryons (BBNS)	0.088		
Metals synthesised in Lyman Break Galaxies			0.035

[a]All entries are for $H_0 = 50$ km s^{-1} Mpc^{-1}; $\Omega_{\rm M} = 1$, $\Omega_\Lambda = 0$.
[b]In units of the closure density $\rho_{\rm crit} = 3.1 \times 10^{11}\, h^2\, M_\odot\, {\rm Mpc}^{-3}$.
[c]In units of solar metallicity (0.0189 by mass).
[d]In units of $\Omega_{Z_\odot} = \Omega_{\rm baryons} \times Z_\odot = 1.7 \times 10^{-3}$.

this census because we still have no idea of their metallicities; potentially they could make a significant contribution to Ω_Z(LBG) because they are so numerous.

Nevertheless, when we add up all the metals which have been measured with some degree of confidence up to now, we find that they account for no more than $\approx 10 - 15\%$ of what we expect to have been produced by $z = 2.5$ (last column of Table 3). Where are these missing metals? Possibly, Ω_Z(DLA) has been underestimated, if the dust associated with the most metal-rich DLAs obscures background QSOs sufficiently to make them drop out of current samples. However, preliminary indications based on the CORALS survey by Ellison et al. (2001) suggest that this may be a relatively minor effect (see also Prochaska & Wolfe 2002). The concordance in the values of Ω_Z(IGM) derived from observations of O VI and C IV absorption in the Lyα forest makes it unlikely that the metallicity of the widespread IGM has been underestimated by a large factor. On the other hand, we do know that Lyman break galaxies commonly drive large scale outflows; it is therefore possible, and indeed likely, that they enrich with metals much larger masses of gas than those seen directly as sites of star formation. This gas and associated metals may be difficult to detect if they are at high temperatures, and yet may make a major contribution to Ω_Z; there are tantalising hints that this could be the case at the present epoch (Tripp, Savage, & Jenkins 2000; Mathur, Weinberg, & Chen 2002).

In concluding this series of lectures, it is clear that while we have made some strides forward towards our goal of charting the chemical history of the universe, our task is far from complete. It is my hope that, stimulated in part by this school, some of the students who have attended it will soon be contributing to this exciting area of observational cosmology as their enter their research careers.

I am very grateful to César Esteban, Artemio Herrero, Rafael García López and Prof. Francisco Sánchez for inviting me to take part in a very enjoyable Winter School, and to the students for their patience and challenging questions. The results described in these lectures were obtained in various collaborative projects primarily with Chuck Stei-

del, Kurt Adelberger, David Bowen, Mark Dickinson, Sara Ellison, Mauro Giavalisco, Samantha Rix and Alice Shapley; I am fortunate indeed to be working with such productive and generous colleagues. Special thanks to Alec Boksenberg and Bernard Pagel for continuing inspiration and for valuable comments on an early version of the manuscript. As can be appreciated from these lecture notes, the measurement of element abundances at high redshifts is a vigorous area of research. In the spirit of the school, I have not attempted to give a comprehensive set of references to all the numerous papers on the subject which have appeared in recent years, as one would in a review. Rather, I have concentrated on the main issues and only given references as pointers for further reading. I apologise for the many excellent papers which have therefore been omitted from the (already long) list of references. Such omissions do not in any way denote criticism on my part of the work in question.

REFERENCES

Adelberger, K.L., & Steidel, C.C. 2000, ApJ, 544, 218

Aguirre, A., Hernquist, L., Schaye, J., Katz, N., Weinberg, D. H., & Gardner, J. 2001, ApJ, 561, 521

Bechtold, J., Crotts, A.P.S., Duncan, R.C., & Fang, Y. 1994, ApJ, 437, L83

Bechtold, J. 2002, in Galaxies at High Redshift, eds. I. Pérez-Fournon, M. Balcells, F. Moreno-Insertis, & F. Sánchez, (Cambridge: Cambridge Univ. Press), p. 131

Binney, J., Gerhard, O., & Silk, J. 2001, MNRAS, 321, 471

Boissier, S., Péroux, C., & Pettini, M. 2002, MNRAS, submitted

Bouché, N., Lowenthal, J.D., Charlton, J.C., Bershady, M.A., Churchill, C.W., & Steidel, C.C. 2001, ApJ, 550, 585

Bouchet, P., Lequeux, J., Maurice, E., Prevot, L., & Prevot-Burnichon, M.L. 1985, A&A, 149, 330

Bruzual, A.G., & Charlot, S. 1993, ApJ, 405, 538

Bunker, B., Ferguson, A., Johnson, R. et al. 2001, in Deep Fields, ESO Astrophysics Symposia, eds. S. Cristiani, A. Renzini, & R.E. Williams, (Berlin:Springer), 330

Carswell, R.F., Schaye, J., & Kim, T.S. 2002, ApJ, in press (astro-ph/0204370)

Cen, R., & Ostriker, J.P. 1999, ApJ, 519, L109

Cole, S., Norberg, P., Baugh, C.M., et al. 2001, MNRAS, 326, 255

Cowie, L.L., Songaila, A., Kim, T.S., & Hu, E.M. 1995, AJ, 109, 1522

Croft, R.A.C., Weinberg, D.H., Bolte, M. et al. 2002, ApJ, submitted (astro-ph/0012324)

Davé, R., Hellsten, U., Hernquist, L., Katz, N. & Weinberg, D.H. 1998, ApJ, 509, 661

Diplas, A., & Savage, B.D. 1994, ApJ, 427, 274

Edmunds, M.G., & Pagel, B.E.J. 1978, MNRAS, 185, 77P

Efstathiou, G. 2000, MNRAS, 317, 697

Ellingson, E., Yee, H.K.C., Bechtold, J., & Elston, R. 1996, ApJ, 466, L71

Ellison, S.L. 2000, Ph.D. Thesis, University of Cambridge

Ellison, S.L., Lewis, G.F., Pettini, M., Chaffee, F.H., & Irwin, M.J. 1999, ApJ, 520, 456

Ellison, S.L., Songaila, A., Schaye, J., Cowie, L.L., & Pettini, M. 2000, AJ, 120, 1175

Ellison, S.L., Yan, L., Hook, I.M., Pettini, M., Wall, J.V., & Shaver, P. 2001, A&A, 379, 393

Fall, S.M. 1996, in The Hubble Space Telescope and the High Redshift Universe, eds. N. Tanvir, A. Aragon-Salamanca, & J.V. Wall (Singapore: World Scientific), 303

Fuhrmann, K. 1998, A&A, 338, 161

Garnett, D.R., Shields, G.A., Peimbert, M., et al. 1999, ApJ, 513, 168

Giavalisco, M., Steidel, C.C., & Macchetto, F.D. 1996, ApJ, 470, 189

Gilmore, G., & Wyse, R.F.G. 1991, ApJ, 367, L55

Grevesse, N., & Sauval, A.J. 1998, Space Sci Rev, 85, 161

Hamann, F., & Ferland, G. 1999, ARA&A, 37, 487

Haehnelt, M.G., Steinmetz, M., & Rauch, M. 1998, ApJ, 495, 647

Heckman, T.M. 2001, in ASP Conf. Ser., Gas and Galaxy Evolution, ASP Conference Proceedings, Vol. 240, eds. J.E. Hibbard, M.P. Rupen, & J.H. van Gorkom, (San Francisco:ASP), 345

Henry, R.B.C., Edmunds, M.G., & Köppen, J. 2000, ApJ, 541, 660

Hernquist, L., Katz, N., Weinberg, D.H., & Miralda-Escudé, J. 1996, ApJ, 457, L51

Holweger, H. 2001, in Solar and Galactic Composition, ed. R.F. Wimmer-Schweingruber, American Institute of Physics Conference proceedings, 598, 23

Kanekar, N., & Chengalur, J.N. 2001, A&A, 369, 42

Kennicutt, R.C. 1998a, in ASP Conf. Ser. 142, The Stellar Initial Mass Function, ed. G. Gilmore & D. Howell (San Francisco: ASP), 1

Kennicutt, R.C. 1998b, in The Next Generation Space Telescope: Science Drivers and Technological Challenges, 34th Liège Astrophysics Colloquium, 81

Krauss, L.M., & Chaboyer, B. 2001, Nature, submitted (astro-ph/0111597)

Kulkarni, V., & Fall, S.M., 2002, ApJ, submitted

Laird, J.B., Rupen, M.P., Carney, B.W., & Latham, D.W. 1988, AJ, 96, 1908

Lanzetta, K.M. 1993, in The Environment and Evolution of Galaxies, eds. J.M. Shull & H.A. Thronson, (Dordrecht: Kluwer), 237

Larsen, T.I., Sommer-Larsen, J., & Pagel, B.E.J. 2001, MNRAS, 323, 555

Ledoux, C., Bergeron, J., & Petitjean, P. 2002, A&A, 385, 802

Ledoux, C., Petitjean, P., Bergeron, J., Wampler, E.J., & Srianand, R. 1998, A&A, 337, 51

Leitherer, C., Schaerer, D., Goldader, J.D., et al. 1999, ApJS, 123, 3

Leitherer, C., Leão, J.R.S., Heckman, T.M., Lennon, D.J., Pettini, M., & Robert, C. 2001, ApJ, 550, 724

Madau, P., Ferguson, H.C., Dickinson, M.E., Giavalisco, M., Steidel, C.C., & Fruchter, A. 1996, MNRAS, 283, 1388

Madau, P., Ferrara, A., & Rees, M.J. 2001, ApJ, 555, 92

Madau, P., & Shull, J.M. 1996, ApJ, 457, 551

Mathur, S., Weinberg, D.H., & Chen, X. 2002, ApJ, submitted (astro-ph/0206121)

Matteucci, F., & Recchi, S. 2001, ApJ, 558, 351

McGaugh, S. 1991, ApJ, 380, 140

McWilliam, A., Preston, G.W., Sneden, C., & Searle, L. 1995, AJ, 109, 2757

Meyer, D.M., Welty, D.E., & York, D.G. 1989, ApJ, 343, L37

Meynet, G. & Maeder, A. 2002, A&A, 381, L25

Miralda-Escudé, J., & Rees, M.J. 1997, ApJ, 478, L57

Mo, H.J., Mao, S., & White, S.D.M. 1999, MNRAS, 304, 175

Molaro, P., Bonifacio, P., Centurión, M., D'Odorico, S., Vladilo, G., Santin, P., & Di Marcantonio, P. 2000, ApJ, 541, 54

Molaro, P., Levshakov, S.A., D'Odorico, S., Bonifacio, P., & Centurión, M. 2001, ApJ, 549, 90

Møller, P., Warren, S.J., Fall, S.M., Fynbo, J.U., & Jakobsen, P. 2002, ApJ, in press (astro-ph/0203361)

Nagamine, K., Fukugita, M., Cen, R., & Ostriker, J.P. 2001, ApJ, 558, 497

Pagel, B.E.J. 2002, in ASP Conf. Series 253, Chemical Enrichment of Intracluster and Intergalactic Medium, eds. R. Fusco-Femiano & F. Matteucci, (San Francisco: ASP), 489

Pagel, B.E.J., Edmunds, M.G., Blackwell, D.E., Chun, M.S., & Smith, G. 1979, MNRAS, 189, 95

Pagel, B.E.J., & Tautvaisiene, G. 1998, MNRAS, 299, 535

Papovich, C., Dickinson, M., & Ferguson, H.C. 2001, ApJ, 559, 620

Pei, Y.C., Fall, S.M., & Bechtold, J. 1991, ApJ, 378, 6

Pei, Y.C., Fall, S.M., & Hauser, M.G. 1999, ApJ, 522, 604

Penton, S.V., Shull, J.M., & Stocke, J.T. 2000, ApJ, 544, 150

Péroux, C., McMahon, R.G., Storrie-Lombardi, L.J., & Irwin, M.J. 2002, MNRAS, submitted (astro-ph/0107045)

Petitjean, P., & Bergeron, J. 1994, A&A, 283, 759

Petitjean, P., Srianand, R., & Ledoux, C. 2000, A&A, 364, L26

Pettini, M. 2001, in Gaseous Matter in Galaxies and Intergalactic Space, ed. R. Ferlet, M. Lemoine, J.M. Desert, & B. Raban (Frontier Group), 315

Pettini, M., Boksenberg, A., & Hunstead, R.W. 1990, ApJ, 348, 48

Pettini, M., & Bowen, D.V. 2001, ApJ, 560, 41

Pettini, M., Ellison, S. L., Bergeron, J., & Petitjean, P. 2002a, A&A, in press (astro-ph/0205472)

Pettini, M., Ellison, S. L., Steidel, C. C., & Bowen, D. V. 1999, ApJ, 510, 576

Pettini, M., Ellison, S. L., Steidel, C. C., Shapley, A. E., & Bowen, D. V. 2000a, ApJ, 532, 65

Pettini, M., Lipman, K., & Hunstead, R.W. 1995, ApJ, 451, 100

Pettini, M., King, D.L., Smith, L.J., & Hunstead, R.W. 1997a, ApJ, 478, 536

Pettini, M., Rix, S.A., Steidel, C.C., Adelberger, K.L., Hunt, M.P., & Shapley, A.E. 2002b, ApJ, 569, 742

Pettini, M., Shapley, A.E., Steidel, C.C., Cuby, J.G., Dickinson, M., Moorwood, A.F.M., Adelberger, K.L., & Giavalisco, M. 2001, ApJ, 554, 981

Pettini, M., Smith, L.J., Hunstead, R.W., & King, D.L. 1994, ApJ, 426, 79

Pettini, M., Smith, L.J., King, D.L. & Hunstead, R.W. 1997b, ApJ, 486, 665

Pettini, M., Steidel, C.C., Adelberger, K.L., Dickinson, M., & Giavalisco, M. 2000b, ApJ, 528, 96

Prochaska, J.X., Gawiser, E., & Wolfe A. 2001, ApJ, 552, 99

Prochaska, J.X., Gawiser, E., & Wolfe A., et al. 2002, AJ, 123, 2206

Prochaska, J.X., & Wolfe A. 1998, ApJ, 507, 113

Prochaska, J.X., & Wolfe A. 1999, ApJS, 121, 369

Prochaska, J.X., & Wolfe A. 2002, ApJ, 566, 68

Rao, S.M., & Turnshek, D.A. 2000, ApJS, 130, 1

Rauch, M. 1998, ARA&A, 36, 267

Rosenberg, J., & Schneider, S. 2002, ApJ, submitted (astro-ph/0202216)

Ryan, S.G., Norris, J.E., & Beers, T.C. 1996, ApJ, 471, 254

Sargent, W.L.W., Young, P.J., Boksenberg, A., & Tytler, D. 1980, ApJS, 42, 41

Savage, B.D., & Sembach, K.R. 1996, ARA&A, 34, 279

Schaye, J., Rauch, M., Sargent, W.L.W., & Kim, T.S. 2000, ApJ, 541, L1

Seitz, S., Saglia, R.P., Bender, R., Hopp, U., Belloni, P., & Ziegler, B. 1998, MNRAS, 298, 945

Shapley, A.E., Steidel, C.C., Adelberger, K.L., Dickinson, M., Giavalisco, M., &

Pettini, M. 2001, ApJ, 562, 95

Sneden, C., Gratton, R.G., & Crocker, D.A. 1991, A&A, 246, 354

Songaila, A. 1997, ApJ, 490, L1

Songaila, A. 2001, ApJ, 561, L153

Songaila, A., & Cowie, L.L. 2002, AJ, 123, 2183

Steidel, C.C. 1993, in The Environment and Evolution of Galaxies, eds. J.M. Shull & H.A. Thronson, (Dordrecht: Kluwer), 263

Steidel, C.C. 2000, in Discoveries and Research Prospects from 8- to 10-Meter-Class Telescopes, ed. J. Bergeron, Proc. SPIE Vol. 4005, 22

Steidel, C.C., Adelberger, K.L., Giavalisco, M., Dickinson, M., & Pettini, M. 1999, ApJ, 519, 1

Steidel, C.C., Dickinson, M., Meyer, D.M., Adelberger, K. L., & Sembach, K.R. 1997, ApJ, 480, 568

Steidel, C.C., Dickinson, M., & Persson, S.E. 1994, ApJ, 437, L75

Steidel, C.C., Giavalisco, M., Pettini, M., Dickinson, M., & Adelberger, K. L. 1996, ApJ, 462, L17

Steidel, C.C., Pettini, M., & Adelberger, K.L. 2001, ApJ, 546, 665

Steidel, C.C., Pettini, M., & Hamilton, D. 1995, AJ, 110, 2519

Storrie-Lombardi, L.J., & Wolfe, A.M. 2000, ApJ, 543, 552

Teplitz, H.I., McLean, I.S., Becklin, E.E., et al. 2000, ApJ, 533, L65

Tripp, T.M., Savage, B.D., & Jenkins, E.B. 2000, ApJ, 534, L1

Turner, M.S. 2002, in Proceedings of the XXth International Symposium on Photon and Lepton Interactions, in press (astro-ph/0202007)

Tytler, D. 1987, ApJ, 321, 49

Tytler, D., Fan, X.-M., Burles, S., Cottrell, L., Davis, C., Kirkman, D., & Zuo, L. 1995, QSO Absorption Lines, ed. G. Meylan, (Garching, ESO), 289

Tytler, D., O'Meara, J.M., Suzuki, N., & Lubin, D. 2000, Physica Scripta T, 85, 12

Vladilo, G. 2002a, ApJ, 569, 295

Vladilo, G. 2002b, A&A, in press (astro-ph/0206048)

Vladilo, G., Centurión, M., Bonifacio, P., & Howk, J.C. 2001, ApJ, 557, 1007

Weinberg, D.H., Katz, N., & Hernquist, L. 1998, in ASP Conf. Series 128, Origins, ed. C.E. Woodward, J.M. Shull, & H.A. Thronson, (San Francisco: ASP), 21

Wheeler, J.C., Sneden, C., & Truran, J.W. 1989, ARA&A, 27, 279

Wolfe, A. M., Turnshek, D. A., Smith, H. E., & Cohen, R. D. 1986, ApJS, 61, 249

Wolfire, M.G., Hollenbach, D., McKee, C.F., Tielens, A.G.G.M., & Bakes, E.L.O. 1995, ApJ, 443, 152

Wyse, R.F.G., & Gilmore, G. 1995, AJ, 110, 2771

Yee, H.K.C., Ellingson, E., Bechtold, J., Carlberg, R.G., & Cuillandre, J.-C. 1996, AJ, 111, 1783